





Present and future constraints on flavor-dependent long-range interactions of high-energy astrophysical neutrinos

Sanjib Kumar Agarwalla, ^{a,b,c} Mauricio Bustamante, ^d Sudipta Das ^{a,b} and Ashish Narang ^a

^a*Institute of Physics, Sachivalaya Marg, Sainik School Post, Bhubaneswar 751005, India*

^b*Homi Bhabha National Institute, Training School Complex, Anushakti Nagar, Mumbai 400094, India*

^c*Department of Physics & Wisconsin IceCube Particle Astrophysics Center, University of Wisconsin, Madison, WI 53706, U.S.A.*

^d*Niels Bohr International Academy, Niels Bohr Institute, University of Copenhagen, DK-2100 Copenhagen, Denmark*

E-mail: sanjib@iopb.res.in, mbustamante@nbi.ku.dk, sudipta.d@iopb.res.in, ashish.narang@iopb.res.in

ABSTRACT: The discovery of new, flavor-dependent neutrino interactions would provide compelling evidence of physics beyond the Standard Model. We focus on interactions generated by the anomaly-free, gauged, abelian lepton-number symmetries, specifically $L_e - L_\mu$, $L_e - L_\tau$, and $L_\mu - L_\tau$, that introduce a new matter potential sourced by electrons and neutrons, potentially impacting neutrino flavor oscillations. We revisit, revamp, and improve the constraints on these interactions that can be placed via the flavor composition of the diffuse flux of high-energy astrophysical neutrinos, with TeV–PeV energies, i.e., the proportion of ν_e , ν_μ , and ν_τ in the flux. Because we consider mediators of these new interactions to be ultra-light, lighter than 10^{-10} eV, the interaction range is ultra-long, from km to Gpc, allowing vast numbers of electrons and neutrons in celestial bodies and the cosmological matter distribution to contribute to this new potential. We leverage the present-day and future sensitivity of high-energy neutrino telescopes and of oscillation experiments to estimate the constraints that could be placed on the coupling strength of these interactions. We find that, already today, the IceCube neutrino telescope demonstrates potential to constrain flavor-dependent long-range interactions significantly better than existing constraints, motivating further analysis. We also estimate the improvement

in the sensitivity due to the next-generation neutrino telescopes such as IceCube-Gen2, Baikal-GVD, KM3NeT, P-ONE, and TAMBO.

KEYWORDS: Neutrino Mixing, New Gauge Interactions, New Light Particles, Non-Standard Neutrino Properties

ARXIV EPRINT: [2305.03675](https://arxiv.org/abs/2305.03675)

Contents

1	Introduction	1
2	New long-range, lepton-number neutrino interactions	4
2.1	New lepton-number symmetries: $L_e - L_\mu$, $L_e - L_\tau$, and $L_\mu - L_\tau$	4
2.2	Long-range neutrino interactions	6
2.3	Neutrino flavor-transition probabilities	11
3	High-energy astrophysical neutrinos	12
3.1	Overview	12
3.2	Neutrino detection and flavor composition	14
3.3	Flavor composition of high-energy astrophysical neutrinos	16
3.4	Analysis choices	16
4	Statistical analysis and results	18
4.1	Statistical analysis	18
4.2	Results	20
5	Future improvements	23
6	Summary and outlook	25
A	Interaction potential under the $L_\mu - L_\tau$ symmetry	26
B	Evolution of the modified mixing angles with long-range potential	27
C	Reinterpretation of Super-Kamiokande NSI limits	27
D	Additional results under the $L_e - L_\tau$ symmetry	28
E	Results assuming inverted neutrino mass ordering	30
F	Table of limits on the long-range potential	36

1 Introduction

The high-energy astrophysical neutrinos discovered by the IceCube neutrino telescope [1–8] provide unprecedented potential to explore high-energy fundamental physics [8–13]. Because they reach energies in the TeV–PeV range, they are sensitive to possible new physics at energy scales beyond the reach of terrestrial colliders. Because they travel Gpc-scale distances — essentially the size of the observable Universe — minute new-physics effects,

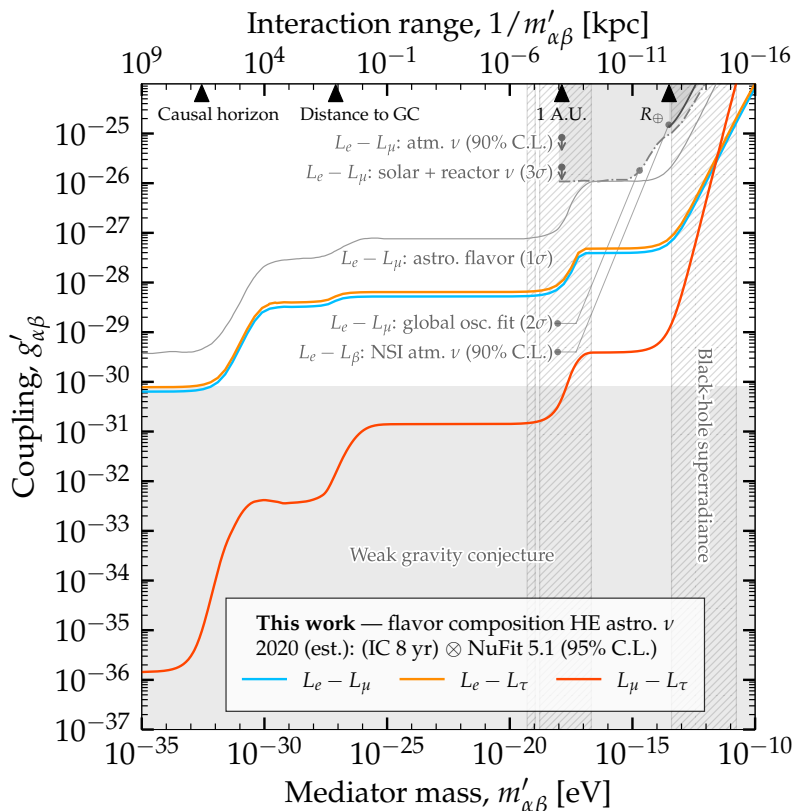


Figure 1. *Estimated present-day upper limits on the coupling strength, $g'_{\alpha\beta}$, of the new boson, $Z'_{\alpha\beta}$, with mass $m'_{\alpha\beta}$, that mediates flavor-dependent long-range neutrino interactions. Our results are based on estimates of the measurement of flavor composition of high-energy astrophysical neutrinos in IceCube using 8 years of data [15] (through-going muons plus HESE, see section 3) and on present-day uncertainties in the neutrino mixing parameters [16, 17], assuming normal neutrino mass ordering. Limits are on neutrino-electron interactions, under the $L_e - L_\mu$ and $L_e - L_\tau$ symmetries, and on neutrino-neutron interactions, under the $L_\mu - L_\tau$ symmetry. For the latter, we assume a $Z'_{\mu\tau}$ - Z mixing strength of $(\xi - \sin\theta_W\chi) = 5 \times 10^{-24}$ [18]. Existing limits are from a recent global oscillation fit [19], atmospheric neutrinos [20], solar and reactor neutrinos [21], and non-standard interactions (NSI) [22–24]. For comparison, we show the proof-of-principle sensitivity (1σ) based on 2015 IceCube flavor-composition measurements [25] from ref. [26]. Indirect limits [27] are from black-hole superradiance (90% C.L.) [28] and the weak gravity conjecture [29], assuming a lightest neutrino mass of 0.01 eV. Figures 8 and 12 show projections for the year 2040; figure 16 shows results assuming inverted mass ordering. See section 4.2 for details. Our results show that limits obtained from present-day flavor-composition measurements may improve significantly on existing ones.*

ordinarily undetectable, may accumulate en route to Earth and become detectable. (They also provide unique insight into the most energetic astrophysical sources [8, 13, 14].) We gear this potential to far-reaching studies of new, long-range neutrino interactions.

Presently, theory and experiment leave room for the possibility that neutrinos undergo interactions beyond the Standard Model weak interactions that would have gone undetected so far. In particular, new interactions that affect different neutrino flavors dif-

ferently may modify neutrino oscillations, and so may be tested in oscillation experiments that use neutrinos from a variety of sources, natural and man-made. References [20, 21] pioneered the idea of introducing such flavor-dependent interactions by gauging native global lepton-number symmetries of the Standard Model, generated by $L_\alpha - L_\beta$, where L_α ($\alpha = e, \mu, \tau$) is the α -flavor lepton number. Doing so introduces new neutrino-matter interactions mediated by a boson that, if light, makes it possible for distant matter to source a long-range potential that affects neutrino oscillation probabilities. Previous works have explored this possibility and placed constraints on the strength of the new interaction using atmospheric neutrinos [20], solar and reactor neutrinos [21], accelerator neutrinos [18, 30], and a global fit to oscillation data [19].

Recently, ref. [26] proposed a new way to probe these interactions using high-energy astrophysical neutrinos. Because the relative contribution of the standard oscillation mechanism, driven by the neutrino masses, falls with neutrino energy, at high energies the contribution from new interactions may become prominent and more easily detectable. By modifying oscillations — in an extreme case, by suppressing flavor transitions — the new interactions would also modify the flavor composition of high-energy astrophysical neutrinos, i.e., the proportion of ν_e , ν_μ , and ν_τ in their flux. IceCube measures the flavor composition of the diffuse flux of high-energy astrophysical neutrinos [25, 31–33] (see also refs. [34–36]) and, though the measurement is challenging, it is a versatile probe of high-energy neutrino physics [8, 10, 11, 13, 37–41] and astrophysics [8, 13, 14]. In particular, the sensitivity to new neutrino interactions stems from looking for characteristic deviations in the flavor composition relative to its expectation under standard oscillations.

Based on this, ref. [26] provided a proof of principle for using the flavor composition measured by IceCube and forecast for its planned upgrade, IceCube-Gen2 [15], to constrain flavor-dependent long-range neutrino-electron interactions generated by gauging the $L_e - L_\mu$ and $L_e - L_\tau$ symmetries. It focused on ultra-light mediators, lighter than 10^{-10} eV, which makes the interaction range ultra-long, from km to Gpc, depending on the mass. As a result, vast numbers of electrons in the Earth, the Moon, the Sun, the Milky Way, and in the distant Universe could source a sizable long-range potential. Yet, while the proof-of-principle prospects in ref. [26] were promising, the statistical methods used therein are not amenable to being generalized to compute sensitivity beyond the 1σ statistical significance.

To address this, we revisit, revamp, and expand the tests of flavor-dependent long-range neutrino interactions based on flavor composition. There are four main improvements in our work. First, we adopt a Bayesian approach to compute constraints, based on the methods from ref. [42]. It allows us to combine consistently the uncertainties in the measurement of the flavor composition in IceCube and other neutrino telescopes, and the uncertainties in the neutrino mixing parameters that drive standard oscillations, and to compute constraints at arbitrary statistical significance. Second, not only do we consider neutrino-electron interactions induced by the $L_e - L_\mu$ and $L_e - L_\tau$ symmetries, as in ref. [26], but also neutrino-neutron interactions induced by the $L_\mu - L_\tau$ symmetry. Third, we study not only the sensitivity of IceCube and IceCube-Gen2, but also the sensitivity achieved by combining them with other neutrino telescopes expected by 2040, Baikal-GVD [43], KM3NeT [44], P-ONE [45], and TAMBO [46]. Fourth, we use projected measurements of the mixing

parameters in upcoming neutrino oscillation experiments, the Deep Underground Neutrino Experiment (DUNE) [47], Hyper-Kamiokande (HK) [48], and the Jiangmen Underground Neutrino Observatory (JUNO) [49], that will shrink the uncertainty on their values.

Figure 1 shows our main results, in the form of upper limits on the coupling strength of the new interactions, conservatively based on approximate present-day flavor-measurement capabilities in IceCube and of uncertainties in the mixing parameters. For mediators lighter than 10^{-18} eV, our estimated upper limits confirm [26] the reach of flavor-composition measurements to test ultra-long-range interactions, now at higher statistical significance. We find that, *already today, high-energy astrophysical neutrinos may be able to constrain flavor-dependent long-range neutrino interactions more strongly than existing limits*. By 2040, our conservative forecast limits, not shown in figure 1, improve marginally (section 4.2), though more power may be reaped from improvements to our analysis that could be afforded by significantly higher detection rates of high-energy neutrinos and precision in the mixing parameters. We point these out later (section 5).

We provide our constraints as approximate, rather than as definitive, since they rely on specific, albeit realistic assumptions on present-day and upcoming experimental capabilities. For instance, they are obtained assuming that measurements of the flavor composition are performed on an astrophysical neutrino spectrum that is a power law $\propto E^{-2.5}$, where E is the neutrino energy. While this is compatible with IceCube observations [25], our results do not account for deviations from this assumption that lie within experimental error, and which could make the spectrum softer (see, e.g., ref. [7]) or harder (see, e.g., ref. [50]). Accounting for this would require deriving the IceCube flavor sensitivity for different choices of the neutrino spectrum, as in ref. [25], which involves combining different data sets that are not available outside the Collaboration. Doing so lies beyond the scope of this paper, but we comment on possible future developments (section 5).

This paper is organized as follows. Section 2 introduces long-range interactions and their effect on neutrino oscillations. Section 3 provides an overview of high-energy astrophysical neutrinos and shows the effect of long-range interactions on their flavor composition. Section 4 presents our statistical methods and results. Section 5 points out future improvements of our analysis. Section 6 summarizes and concludes.

2 New long-range, lepton-number neutrino interactions

2.1 New lepton-number symmetries: $L_e - L_\mu$, $L_e - L_\tau$, and $L_\mu - L_\tau$

The Standard Model (SM), in addition to the gauge group $SU(3)_C \times SU(2)_L \times U(1)_Y$, contains global $U(1)$ symmetries associated to the baryon number and the three lepton numbers, L_e , L_μ , and L_τ . While they cannot be gauged individually without introducing anomalies, certain combinations of them can be; for an extensive list, see ref. [19]. We focus on three well-motivated, anomaly-free symmetries that gauge lepton number differences [51–53]: $U(1)_{L_e - L_\mu}$, $U(1)_{L_e - L_\tau}$, and $U(1)_{L_\mu - L_\tau}$. Each one introduces a new neutral gauge vector boson, $Z'_{e\mu}$, $Z'_{e\tau}$, and $Z'_{\mu\tau}$, that mediates new neutrino interactions [52–54] with electrons and neutrons, as we show below. (The Higgs sector differentiates between different lepton flavors [55]; however, here we focus only on the gauge interactions through

the new boson.) The $L_\alpha - L_\beta$ gauge symmetries and their extensions have been explored in numerous scenarios, including as possible solutions of the Hubble tension [56], of the electron and muon ($g - 2$) anomalies [57–60], considering the new boson to be dark matter [61–63] and as radiation from compact binary systems [64], leptogenesis [65], their influence on muon-beam dumps at the TeV-scale [66], possible production of dark photons at the MUonE experiment [67], and explaining the electron and positron excess in the cosmic-ray flux [68, 69]. However, these studies consider mediators that are heavier than the ones we consider here, and couplings (see below) that are stronger.

The effective neutrino-matter interaction receives three contributions, mediated by the SM Z boson, by the new $Z'_{\alpha\beta}$ boson, and via the mixing between $Z'_{\alpha\beta}$ and Z , i.e.,

$$\mathcal{L}_{\text{eff}} = \mathcal{L}_{\text{SM}} + \mathcal{L}_{Z'} + \mathcal{L}_{\text{mix}} . \quad (2.1)$$

The first term in eq. (2.1), \mathcal{L}_{SM} , is the SM contribution, i.e.,

$$\mathcal{L}_{\text{SM}} = \frac{e}{\sin\theta_W \cos\theta_W} Z_\mu \left[-\frac{1}{2} \bar{l}_\alpha \gamma^\mu P_L l_\alpha + \frac{1}{2} \bar{\nu}_\alpha \gamma^\mu P_L \nu_\alpha + \frac{1}{2} \bar{u} \gamma^\mu P_L u - \frac{1}{2} \bar{d} \gamma^\mu P_L d \right] , \quad (2.2)$$

where e is the unit electric charge, θ_W is the Weinberg angle, l_α and ν_α are, respectively, the charged lepton and neutrino of flavor $\alpha = e, \mu, \text{ or } \tau$, u and d are the up and down quarks, and P_L is the left-handed projection operator. (Equation (2.2), and also eq. (2.4) below, assumes that matter is electrically neutral, i.e., that it contains equal numbers of electrons and protons [18]; this is also what we assume later when computing the new matter potential; see section 2.2.)

The second term in eq. (2.1), $\mathcal{L}_{Z'}$, describes neutrino-matter interactions via the new mediator [18, 19, 52, 53], i.e.,

$$\mathcal{L}_{Z'} = g'_{\alpha\beta} Z'_\sigma (\bar{l}_\alpha \gamma^\sigma l_\alpha - \bar{l}_\beta \gamma^\sigma l_\beta + \bar{\nu}_\alpha \gamma^\sigma P_L \nu_\alpha - \bar{\nu}_\beta \gamma^\sigma P_L \nu_\beta) , \quad (2.3)$$

where $g'_{\alpha\beta}$ ($\alpha, \beta = e, \mu, \tau, \alpha \neq \beta$) is the adimensional coupling constant associated to the $L_\alpha - L_\beta$ gauge symmetry. Because naturally occurring muons and tauons are scarce, we consider this contribution only under $L_e - L_\mu$ and $L_e - L_\tau$, and the corresponding interaction to be sourced only by abundant electrons.

The third term in eq. (2.1), \mathcal{L}_{mix} , contains terms that mix $Z'_{\alpha\beta}$ with Z [18, 70, 71], i.e., $\mathcal{L}_{ZZ'} = -\frac{1}{2} \sin\chi \hat{Z}'_{\mu\nu} \hat{B}^{\mu\nu} + \delta\hat{M}^2 \hat{Z}'_\mu \hat{Z}^\mu$, where $\hat{Z}'_{\mu\nu}$ and $\hat{B}^{\mu\nu}$ are the field strength tensors for $U(1)'$ and $U(1)_Y$, respectively, \hat{Z} and \hat{Z}' are the gauge eigenstates corresponding to the neutral massive gauge bosons of the SM and the new $U(1)'$ gauge symmetry, χ is the kinetic mixing angle, and $\delta\hat{M}^2$ is the squared-mass difference between \hat{Z} and \hat{Z}' . Diagonalizing this Lagrangian redefines the fields in terms of physical states: the photon and two massive bosons, Z and Z' , that are related to \hat{Z} and \hat{Z}' through a new mixing angle ξ [70], i.e., $\mathcal{L}_{ZZ'} \supset (\xi - \sin\theta_W \chi) Z'_\mu Z^\mu$. This introduces a four-fermion neutrino-matter interaction term via $Z-Z'_{\alpha\beta}$ mixing, i.e.,

$$\mathcal{L}_{\text{mix}} = -g'_{\alpha\beta} (\xi - \sin\theta_W \chi) \frac{e}{\sin\theta_W \cos\theta_W} J'_\rho J_3^\rho , \quad (2.4)$$

where $J'_\rho = \bar{\nu}_\alpha \gamma_\rho P_L \nu_\alpha - \bar{\nu}_\beta \gamma_\rho P_L \nu_\beta$ and $J_3^\rho = -\frac{1}{2} \bar{e} \gamma^\rho P_L e + \frac{1}{2} \bar{u} \gamma^\rho P_L u - \frac{1}{2} \bar{d} \gamma^\rho P_L d$. To illustrate the effect of mixing, below we fix the value of the mixing strength to $(\xi - \sin \theta_W \chi) = 5 \times 10^{-24}$ [18], the upper limit for a new interaction whose range is of the order of the distance between the Earth and the Sun [18, 72, 73]. (The upper limit on the mixing strength for an interaction range of the order of the size of the Earth is slightly weaker and allows for larger mixing [18, 72, 73].) Because of our analysis choices, $Z-Z'_{\alpha\beta}$ mixing affects the results only under the $L_\mu - L_\tau$ symmetry; we explain this below.

Figure 2 shows the Feynman diagrams corresponding to the above contributions. Regarding \mathcal{L}_{SM} , because the Z boson is heavy, the SM neutral-current interaction is short-range and significant only in relatively high-density regions such as inside the Earth (which we account for later). Regarding $\mathcal{L}_{Z'}$, it induces new interactions between neutrinos and charged leptons. However, in practice, the scarcity of muons and tauons in Nature means that interactions are sourced only by electrons. As a result, this term in the Lagrangian is active only for the $L_e - L_\mu$ and $L_e - L_\tau$ symmetries. Regarding \mathcal{L}_{mix} , it induces interactions between neutrinos and electrons, protons, and neutrons. Under the $L_\mu - L_\tau$ symmetry, this is the dominant contribution; its size depends on the value of the mixing strength (see above). Further, for a macroscopic collection of ordinary matter, like the ones we consider below, the contribution of electrons is nullified by the contribution of protons, leaving only neutrons to source the new interaction; see appendix A for details. Under the $L_e - L_\mu$ and $L_e - L_\tau$ symmetries, the relative importance of \mathcal{L}_{mix} vs. $\mathcal{L}_{Z'}$ depends on the value of the mixing strength; to be conservative, we assume no mixing for these two symmetries.

In summary, under the $L_e - L_\mu$ and $L_e - L_\tau$ symmetries, the new neutrino interaction is via $\mathcal{L}_{Z'}$ and is sourced by electrons only. Under the $L_\mu - L_\tau$ symmetry, it is via \mathcal{L}_{mix} and is sourced by neutrons only. Under all symmetries, \mathcal{L}_{SM} acts only inside the Earth.

2.2 Long-range neutrino interactions

A neutrino separated by a distance d from a collection of N_e electrons, under $L_e - L_\mu$ and $L_e - L_\tau$, or of N_n neutrons, under $L_\mu - L_\tau$, experiences a Yukawa potential of

$$V_{\alpha\beta} = \mathcal{G}_{\alpha\beta} \frac{e^{-m'_{\alpha\beta} d}}{4\pi d} \times \begin{cases} N_e, & \text{for } \alpha, \beta = e, \mu \text{ or } e, \tau \\ N_n, & \text{for } \alpha, \beta = \mu, \tau \end{cases}, \quad (2.5)$$

where $m'_{\alpha\beta}$ is the mass of the $Z'_{\alpha\beta}$ boson and the coupling strength is

$$\mathcal{G}_{\alpha\beta} = \begin{cases} g_{e\mu}^2, & \text{for } \alpha, \beta = e, \mu \\ g_{e\tau}^2, & \text{for } \alpha, \beta = e, \tau \\ g'_{\mu\tau} (\xi - \sin \theta_W \chi) \frac{e}{4 \sin \theta_W \cos \theta_W}, & \text{for } \alpha, \beta = \mu, \tau \end{cases}. \quad (2.6)$$

The range of the interaction is $\sim 1/m'_{\alpha\beta}$; beyond this distance from the source of the potential, it is suppressed due to the mediator mass. Depending on the interaction range, the potential receives contributions from nearby bodies — if the mediator is heavy — or also from distant bodies — if the mediator is light. We consider masses of 10^{-35} – 10^{-10} eV, for which the interaction range is km–Gpc, which encompasses the Earth (\oplus), Moon (☾), Sun

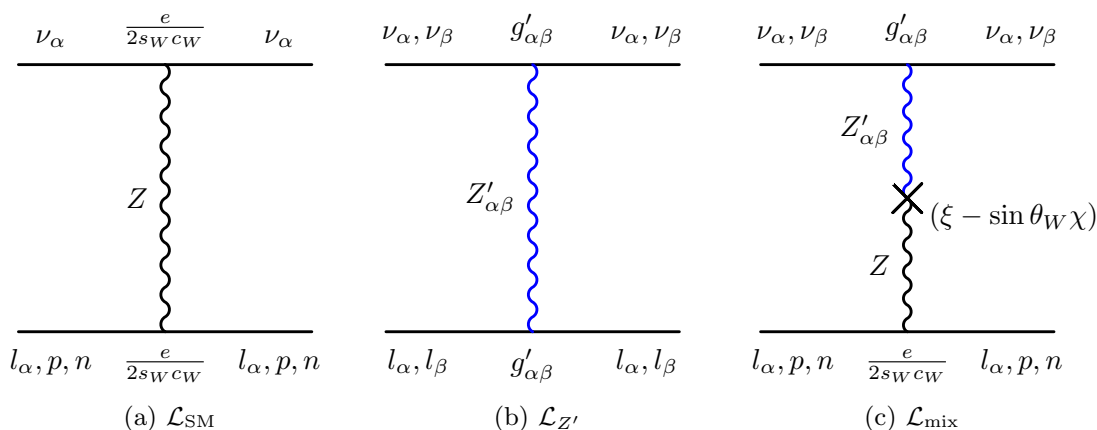


Figure 2. Feynman diagrams for the contributions to the neutrino-matter interaction Lagrangian, eq. (2.1). (a) Neutrino-matter interaction in the Standard Model, mediated by the neutral gauge boson Z . In our analysis, this is important only for neutrinos inside the Earth, where matter densities are high. (b) Neutrino-matter interaction in the $U(1)_{L_\alpha-L_\beta}$ model, mediated by the new $Z'_{\alpha\beta}$ gauge boson. (c) Neutrino-matter interaction via $Z'_{\alpha\beta}$ - Z mixing. In our analysis, for the $L_e - L_\mu$ and $L_e - L_\tau$ symmetries, only diagram (a) (and only inside the Earth) and diagram (b), sourced by electrons, contribute, and we do not consider diagram (c). For the $L_\mu - L_\tau$ symmetry, only diagram (a) (and only inside the Earth) and diagram (c), sourced by neutrons, contribute. See section 2.1 for details.

(\odot), Milky Way (MW) and the cosmological matter distribution (cos). Thus, the potential experienced by neutrinos is the sum of the contributions sourced by each of them, i.e.,

$$V_{\alpha\beta} = V_{\alpha\beta}^{\oplus} + V_{\alpha\beta}^{\odot} + V_{\alpha\beta}^{\odot} + V_{\alpha\beta}^{\text{MW}} + \langle V_{\alpha\beta}^{\text{cos}} \rangle, \quad (2.7)$$

and the relative contribution of each term depends on the value of $m'_{\alpha\beta}$.

We do not compute the changing potential along the underground trajectories of the neutrinos inside the Earth or inside the Sun; see ref. [19] for such treatment. Instead, like ref. [26], we compute the average potential experienced by the neutrinos at their point of detection in IceCube. This approximation is especially valid for mediators lighter than about 10^{-18} eV, for which the interaction range is longer than the Earth-Sun distance (see figure 1), and so all of the electrons and neutrons on the Earth or the Sun contribute to the potential experienced by a neutrino regardless of its position inside them. Below 10^{-18} eV is also where we place limits in an unexplored range of mediator mass.

In what follows, we use eq. (2.5) as a basis to calculate the potential induced by these sources. We adopt the methods introduced in ref. [26] for the $L_e - L_\mu$ and $L_e - L_\tau$ cases. Below, we revisit them, extend them to the $L_\mu - L_\tau$ case, and introduce refinements in the computation of the potential due to solar and cosmological electrons and neutrons. Throughout, we assume that matter is electrically neutral, so that the number of electrons and protons is the same, and that matter is isoscalar, so that the number of electrons and neutrons is the same, except for the Sun and for the cosmological distribution of matter.

The Earth. Astrophysical neutrinos travel inside the Earth from its surface to IceCube, located $d_{\text{IC}} = 1.5$ km underground at the South Pole. Along the way, they undergo long-range interactions with underground electrons or neutrons. Under the $L_\alpha - L_\beta$ symmetry, the potential sourced by them is

$$V_{\alpha\beta}^\oplus = \frac{\mathcal{G}_{\alpha\beta}}{2} \int_0^\pi d\theta_z \int_0^{r_{\text{max}}(\theta_z)} dr r \sin\theta e^{-m'_{\alpha\beta}r} \times \begin{cases} \langle n_{e,\oplus} \rangle_{\theta_z} & , \text{ for } \alpha, \beta = e, \mu \text{ or } e, \tau \\ \langle n_{n,\oplus} \rangle_{\theta_z} & , \text{ for } \alpha, \beta = \mu, \tau \end{cases} \quad (2.8)$$

where θ_z is the zenith angle along which the neutrinos travel, measured from the South Pole, the chord length traveled along this direction is $r_{\text{max}}(\theta_z) = (R_\oplus - d_{\text{IC}}) \cos\theta_z + [(R_\oplus - d_{\text{IC}})^2 \cos^2\theta_z + (2R_\oplus - d_{\text{IC}})d_{\text{IC}}]^{1/2}$, and the radius of the Earth is $R_\oplus = 6371$ km. The average densities of electrons and neutrons along direction θ_z are $\langle n_{e,\oplus} \rangle_{\theta_z} = \langle n_{n,\oplus} \rangle_{\theta_z}$, assuming matter is electrically neutral and isoscalar. To compute them, we adopt the matter density profile of the Preliminary Reference Earth Model [74], and we assume an electron fraction of $Y_e \equiv N_e/(N_e + N_p) = 0.5$. The total number of electrons and neutrons in the Earth is $N_{e,\oplus} \approx N_{n,\oplus} \sim 4 \times 10^{51}$. Because we do not track the propagation of neutrinos inside the Earth and the changing long-range potential that they experience at different points along their trajectories, our treatment is approximate; yet, it allows us explore efficiently the parameter space. For a detailed treatment, see ref. [19].

The Moon and the Sun. We treat the Moon and the Sun as point sources of electrons and neutrons. Under the $L_\alpha - L_\beta$ symmetry, the potential sourced by the Moon is

$$V_{\alpha\beta}^\lrcorner = -\mathcal{G}_{\alpha\beta} \frac{e^{-m'_{\alpha\beta}d_\lrcorner}}{4\pi d_\lrcorner} \times \begin{cases} N_{e,\lrcorner} & , \text{ for } \alpha, \beta = e, \mu \text{ or } e, \tau \\ N_{n,\lrcorner} & , \text{ for } \alpha, \beta = \mu, \tau \end{cases} \quad (2.9)$$

where the distance between the Earth and the Moon is $d_\lrcorner \approx 4 \cdot 10^5$ km, and the number of electrons and neutrons in the Moon is $N_{e,\lrcorner} = N_{n,\lrcorner} \sim 5 \cdot 10^{49}$, assuming the lunar matter is electrically neutral and isoscalar. Similarly, the potential sourced by the Sun is

$$V_{\alpha\beta}^\odot = -\mathcal{G}_{\alpha\beta} \frac{e^{-m'_{\alpha\beta}d_\odot}}{4\pi d_\odot} \times \begin{cases} N_{e,\odot} & , \text{ for } \alpha, \beta = e, \mu \text{ or } e, \tau \\ N_{n,\odot} & , \text{ for } \alpha, \beta = \mu, \tau \end{cases} \quad (2.10)$$

where the distance between the Earth and the Sun is $d_\odot = 1$ A.U., the number of electrons in the Sun is $N_{e,\odot} \sim 10^{57}$, and the number of neutrons in it is $N_{n,\odot} = N_{e,\odot}/4$. Like for Earth, we do not compute the changing long-range matter potential inside the Moon and Sun as neutrinos propagate inside them; for the latter, see ref. [19].

The Milky Way. A neutrino of extragalactic origin traverses the Milky Way before reaching the Earth and may be affected by the long-range potential sourced by Galactic electrons and neutrons. We do not track the propagation of neutrinos inside the Milky Way. Instead, we estimate the effect of long-range interactions by computing the potential experienced by neutrinos at the location of the Earth by integrating the Galactic electron and neutron column densities across all possible neutrino trajectories that have the Earth as the endpoint. Under the $L_\alpha - L_\beta$ symmetry, this is

$$V_{\alpha\beta}^{\text{MW}} = \frac{\mathcal{G}_{\alpha\beta}}{4\pi} \int_0^\infty dr \int_0^\pi d\theta \int_0^{2\pi} d\phi r \sin\theta e^{-m'_{\alpha\beta}r} \times \begin{cases} n_{e,\text{MW}}(r, \theta, \phi) & , \text{ for } \alpha, \beta = e, \mu \text{ or } e, \tau \\ n_{n,\text{MW}}(r, \theta, \phi) & , \text{ for } \alpha, \beta = \mu, \tau \end{cases} \quad (2.11)$$

where the coordinate system is centered at the position of the Earth, 8.33 kpc away from the Galactic Center, and the densities of electrons and neutrons are $n_{e,\text{MW}} = n_{n,\text{MW}}$, assuming matter is electrically neutral and isoscalar. In the Milky Way, $N_{e,\text{MW}} \approx N_{n,\text{MW}} \sim 10^{67}$ electrons and neutrons are contained in stars and cold gas — distributed in a central bulge, a thick disc, and a thin disc — and in hot gas — distributed in a diffuse halo. Following ref. [26], we adopt the “conventional model” from ref. [75] for the matter density of the central bulge, thick disc, and thin disc, and the spherical saturated matter density from ref. [76] for the diffuse halo; figure A1 in ref. [26] shows the total matter distribution.

Cosmological electrons and neutrons. For $m'_{\alpha\beta} \lesssim 10^{-25}$ eV, the dominant contribution to the long-range potential is from the large-scale cosmological distribution of electrons and neutrons. We follow ref. [26] to compute the potential, including the effect of the adiabatic cosmological expansion on the densities of electrons and neutrons; we defer to it for a derivation of the potential. While ref. [26] assumed that the cosmological distribution is isoscalar, we instead account for the fact that, after the recombination epoch, the neutron-to-proton ratio saturates to about 1/7 [77]. Using this and assuming that cosmological matter is electrically neutral, the number of cosmological electrons is seven times higher than that of neutrons. Under the $L_\alpha - L_\beta$ symmetry, the potential at redshift z is

$$V_{\alpha\beta}^{\text{cos}}(z) = \frac{3}{4\pi} \frac{\mathcal{G}_{\alpha\beta}}{m'_{\alpha\beta}{}^2 d_{\text{H}}^3(z)} \left\{ 1 - e^{-m'_{\alpha\beta} d_{\text{H}}(z)} [1 + m'_{\alpha\beta} d_{\text{H}}(z)] \right\} \times \begin{cases} N_{e,\text{cos}}(z) & , \text{ for } \alpha, \beta = e, \mu \text{ or } e, \tau \\ N_{n,\text{cos}}(z) & , \text{ for } \alpha, \beta = \mu, \tau \end{cases} \quad (2.12)$$

where $N_{e,\text{cos}}(z) \simeq 7M_{\text{H}}(z)/(8m_p + 7m_e)$ is the number of electrons, m_p and m_e are the proton and electron mass, respectively, $N_{n,\text{cos}}(z) = N_{e,\text{cos}}(z)/7$ is the number of neutrons, M_{H} is the baryonic mass inside casual horizon (see eq. (16.105) in ref. [78]), and d_{H} is the size of the causal horizon, i.e., the radius of the largest sphere centered on the Earth within which events can be causally connected [79]. We adopt a Λ CDM cosmology with Hubble constant $H_0 = 100h \text{ km s}^{-1} \text{ Mpc}^{-1}$, where $h = 0.673$ [80], the vacuum energy density $\Omega_\Lambda = 0.692$ and the matter density $\Omega_{\text{M}} = 0.308$ [81]. Because we use the diffuse flux of high-energy astrophysical neutrinos, we account for the evolution with redshift of the number density of neutrino sources, ρ_{src} , by averaging the potential over z , i.e.,

$$\langle V_{\alpha\beta}^{\text{cos}} \rangle \propto \int dz \rho_{\text{src}}(z) \frac{dV_{\text{c}}}{dz} V_{\alpha\beta}^{\text{cos}}(z) \quad (2.13)$$

where V_{c} is the comoving volume [82] and ρ_{src} follows the star formation rate [83–85].

Figure 3 shows the total potential, eq. (2.7), as a function of the mediator mass and coupling, for the $L_e - L_\beta$ ($\beta = \mu, \tau$) and $L_\mu - L_\tau$ symmetries. To illustrate its behavior, we show the isocontour for the illustrative value of $V_{\alpha\beta} = 10^{-18}$ eV (which is close to the final constraint that we obtain in section 4.2). As the mass shrinks, the interaction range grows. As a result, the potential isocontour undergoes several step-like transitions, each of which represents the inclusion of the contribution of a more distant collection of electrons and neutrons into the total potential. From $m'_{\alpha\beta} \sim 10^{-10}$ eV to 10^{-18} eV, the

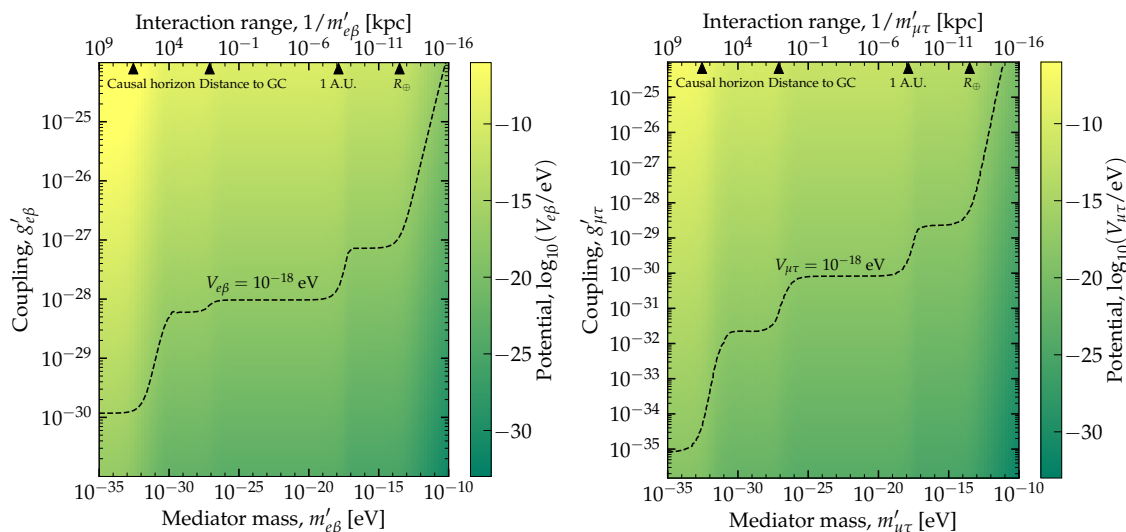


Figure 3. Long-range matter potential, $V_{\alpha\beta}$, experienced by a neutrino at Earth, eq. (2.7). The potential is sourced by electrons and neutrons in the Earth, Moon, Sun, Milky Way, and the distant Universe as a function of the mass and adimensional coupling of the new U(1) gauge symmetry. *Left:* for the $L_e - L_\beta$ symmetries ($\beta = \mu, \tau$), sourced by electrons. *Right:* for the $L_\mu - L_\tau$ symmetry, sourced by neutrons. Isocontours are drawn at the illustrative values of $V_{e\beta} = V_{\mu\tau} = 10^{-18}$ eV. (For the $L_\mu - L_\tau$ symmetry, values of the coupling run lower due to the mixing between the new mediator and the SM Z boson.) The step-like transitions in the potential signal the onset of contributions from sources of electrons and neutrons located at different distances relative to the interaction range. See section 2.2 for details.

potential is dominated by the Earth, with a minor contribution from the Moon. The step at $m'_{\alpha\beta} \sim 10^{-18}$ eV represents the inclusion of the potential sourced by the Sun, which becomes dominant. Because the Sun contains far more electrons and neutrons than the Earth and the Moon, a smaller coupling is enough to achieve the same potential. The step at $m'_{\alpha\beta} \sim 10^{-27}$ eV represents the onset of dominance of Milky-Way electrons and neutrons, which far outnumber those in the Sun, and are concentrated in the Galactic Center. The last step, at $m'_{\alpha\beta} \sim 10^{-33}$ eV, represents the onset of the dominance of cosmological distribution of electrons and neutrons, which far outnumber those in the Milky Way.

For the $L_\mu - L_\tau$ case, figure 3 shows that smaller couplings are needed to achieve the same illustrative value of the potential because it scales $\propto g'_{\mu\tau}$, rather than $\propto g'_{e\beta}{}^2$, as in the $L_e - L_\mu$ and $L_e - L_\tau$ cases; see eq. (2.6). In our work, including in figure 3, for the $L_\mu - L_\tau$ case we fixed the $Z'_{\mu\tau} - Z$ mixing strength, $(\xi - \sin\theta_W\chi)$, to its maximum allowed value (see section 2.1). Decreasing or increasing the mixing strength would shift the potential isocontour in figure 3 up or down, respectively.

2.3 Neutrino flavor-transition probabilities

In the presence of the new $L_\alpha - L_\beta$ gauge symmetry, the Hamiltonian that drives neutrino propagation, written in the flavor basis, is

$$\mathbf{H} = \mathbf{H}_{\text{vac}} + \mathbf{V}_{\text{mat}} + \mathbf{V}_{\alpha\beta} . \quad (2.14)$$

The contributions on the right-hand side describe, respectively, oscillations in vacuum, standard neutrino-matter interactions, and the new neutrino-matter interactions.

Oscillations in vacuum are driven by

$$\mathbf{H}_{\text{vac}} = \frac{1}{2E} \mathbf{U} \text{diag}(0, \Delta m_{21}^2, \Delta m_{31}^2) \mathbf{U}^\dagger , \quad (2.15)$$

where E is the neutrino energy, $\Delta m_{31}^2 \equiv m_3^2 - m_1^2$, and $\Delta m_{21}^2 \equiv m_2^2 - m_1^2$ are the atmospheric and solar mass-squared splittings, respectively, m_i the mass of the ν_i mass eigenstate, and \mathbf{U} is the Pontecorvo-Maki-Nakagawa-Sakata (PMNS) mixing matrix, parameterized as a product of three rotation matrices, i.e., $R(\theta_{23})R(\theta_{13}, \delta_{\text{CP}})R(\theta_{12})$, where θ_{ij} ($i, j = 1, 2, 3$) are three mixing angles and δ_{CP} is the Dirac CP-violating phase. Under normal mass ordering (NMO), where $m_1 < m_2 < m_3$, the present-day best-fit values of the mixing parameters from the global oscillation analysis of refs. [16, 17] are: $\theta_{23} = 42.1^\circ$, $\theta_{13} = 8.62^\circ$, $\theta_{12} = 33.45^\circ$, $\delta_{\text{CP}} = 230^\circ$, $\Delta m_{31}^2 = 2.51 \times 10^{-3} \text{ eV}^2$, and $\Delta m_{21}^2 = 7.42 \times 10^{-5} \text{ eV}^2$. Below, in figures 4 and 10, we adopt these values to illustrate the effect of the new interaction on the neutrino flavor-transition probabilities. Later, in our statistical analysis, we let their values float within their present-day and future predicted allowed ranges.

In eq. (2.14), the contribution of the SM potential from coherent forward neutrino scattering on electrons is

$$\mathbf{V}_{\text{mat}} = \text{diag}(V_{\text{CC}}, 0, 0) , \quad (2.16)$$

where $V_{\text{CC}} = \sqrt{2}G_F \langle n_{e,\oplus} \rangle_{\theta_z}$ is the charged-current neutrino-electron interaction potential and G_F is the Fermi constant. In our calculations, this contribution is relevant only inside Earth, where matter densities are high. The potential above is for neutrinos; for antineutrinos, it flips sign, i.e., $\mathbf{V}_{\text{mat}} \rightarrow -\mathbf{V}_{\text{mat}}$.

Finally, in eq. (2.14) the contribution from the new matter interaction is

$$\mathbf{V}_{\alpha\beta} = \begin{cases} \text{diag}(V_{e\mu}, -V_{e\mu}, 0), & \text{for } \alpha, \beta = e, \mu \\ \text{diag}(V_{e\tau}, 0, -V_{e\tau}), & \text{for } \alpha, \beta = e, \tau \\ \text{diag}(0, V_{\mu\tau}, -V_{\mu\tau}), & \text{for } \alpha, \beta = \mu, \tau \end{cases} , \quad (2.17)$$

where $V_{\alpha\beta}$ is the potential, calculated using eq. (2.7). Depending on the mediator mass, it is sourced by nearby and faraway sources of electrons and neutrons. The potential above is for neutrinos; for antineutrinos, it flips sign, i.e., $\mathbf{V}_{\alpha\beta} \rightarrow -\mathbf{V}_{\alpha\beta}$.

The $\nu_\alpha \rightarrow \nu_\beta$ flavor-transition probability associated to the Hamiltonian, eq. (2.14), is

$$P_{\alpha\beta} = \left| \sum_{i=1}^3 U_{\alpha i}^m \exp \left[-\frac{\Delta \tilde{m}_{i1}^2 L}{2E} \right] U_{\beta i}^{m*} \right|^2 , \quad (2.18)$$

where L is the distance traveled by the neutrino from its point of production to the Earth, $\Delta\tilde{m}_{ij}^2 \equiv \tilde{m}_i^2 - \tilde{m}_j^2$, with $\tilde{m}_i^2/2E$ the eigenvalues of the Hamiltonian, and \mathbf{U}^m is the matrix that diagonalizes the Hamiltonian, parameterized like the PMNS matrix, but in terms of new mixing parameters $\theta_{23}^m, \theta_{13}^m, \theta_{12}^m, \delta_{\text{CP}}^m$. In appendix B, we show the evolution of the three modified mixing angles with the long-range potential. The flavor-transition probability is oscillatory, but for high-energy neutrinos that travel cosmological-scale distances, like the ones we consider, the oscillations are rapid, i.e., $\Delta\tilde{m}_{ij}^2 L/(2E) \gg 1$. Given the limited energy resolution of neutrino telescopes, they are only sensitive to the average probability,

$$\bar{P}_{\alpha\beta} = \sum_{i=1}^3 |U_{\alpha i}^m|^2 |U_{\beta i}^m|^2. \quad (2.19)$$

We use this expression to produce all our results below. Under standard oscillations, i.e., when $V_{\alpha\beta} = 0$, the average oscillation probability loses its dependence on neutrino energy. In contrast, in the presence of the long-range interactions, it retains the energy dependence via the interplay of the vacuum and potential contributions to the Hamiltonian, eq. (2.14).

Figure 4 shows average oscillation probabilities as functions of the potential $V_{\alpha\beta}$, computed for a fixed neutrino energy of 100 TeV, representative of high-energy astrophysical neutrinos. In what follows, we focus on the probabilities under the $L_e - L_\mu$ symmetry. Figure 4 shows that for low values of the potential, i.e., $V_{\alpha\beta} \ll \Delta m_{ij}^2/(2E)$, oscillations are standard. Deviations start to appear when the potential becomes comparable to the Hamiltonian in vacuum, i.e., $V_{\alpha\beta} \approx 10^{-20}$ eV. For neutrinos, sharp features — dips or peaks — appear at $V_{e\mu} \approx 10^{-17}$ eV in the $\nu_e \rightarrow \nu_\beta$ ($\beta = e, \mu, \tau$) probabilities, reflecting that $\theta_{13}^m \approx 45^\circ$ (see appendix B), which maximizes U_{e3}^m and makes flavor transitions resonant. At $V_{e\mu} \approx 10^{-19}$ eV, less prominent features reflect that $\theta_{12}^m = 45^\circ$; they are less prominent because in vacuum $\theta_{12} \approx 45^\circ$ already. Similar features appear in the $\nu_\mu \rightarrow \nu_\tau$ and $\nu_\tau \rightarrow \nu_\tau$ probabilities, for analogous reasons. For large values of the potential, i.e., $V_{\alpha\beta} \gg 10^{-17}$ eV, the term $\mathbf{V}_{\alpha\beta}$ dominates the Hamiltonian and, because it is diagonal, it suppresses flavor transitions. For $L_e - L_\tau$, shown in figure 10, the flavor-transition probabilities are similar to $L_e - L_\mu$. Figure 4 shows that, for $L_\mu - L_\tau$, no resonance due to θ_{13}^m occurs neither for neutrinos nor antineutrinos because θ_{13}^m never reaches 45° , but there is a small dip or jump in the probabilities around $V_{\mu\tau} \approx 10^{-18}$ eV, due to resonant θ_{12}^m .

In the main text, we produce results assuming normal neutrino mass ordering, motivated by recent hints from global oscillation fits [16, 17, 86–88]. For antineutrinos, the sharp features above do not appear because θ_{13}^m and θ_{12}^m never become resonant under normal neutrino ordering. However, they do appear under inverted mass ordering, because Δm_{31}^2 is negative; see appendix E.

3 High-energy astrophysical neutrinos

3.1 Overview

High-energy astrophysical neutrinos, discovered by IceCube in 2013 [1, 2], have the highest neutrino energies detected so far, between tens of TeV to a few PeV [7, 50]. The origin of the

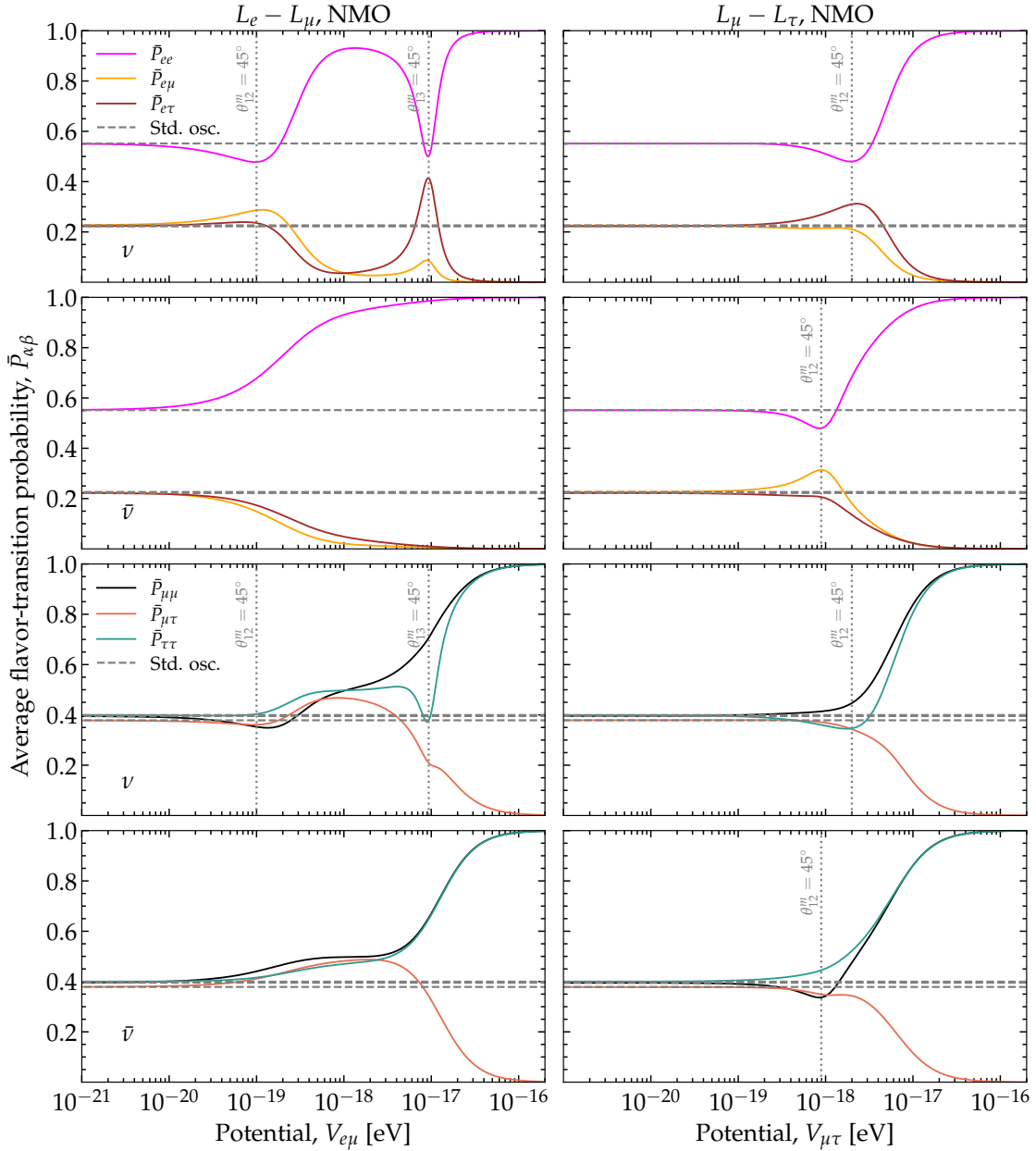


Figure 4. Average flavor-transition probabilities, eq. (2.19), as functions of the new matter potential induced by the U(1) gauge symmetries $L_e - L_\mu$ (left column) and $L_\mu - L_\tau$ (right column). Probabilities are for neutrinos and antineutrinos, at a fixed energy of 100 TeV, assuming normal mass ordering (NMO). The features in the probabilities are due to resonances induced by the new potential. Vertical lines mark the values of the potential for which θ_{12}^m and θ_{13}^m become resonant. Probabilities under standard oscillations (“Std. osc.”), i.e., for $V_{\alpha\beta} = 0$, are shown for comparison. The mixing parameters are fixed at their present-day best-fit values from NuFit 5.1 [16, 17]. Appendix D contains results for $L_e - L_\tau$; they are similar to $L_e - L_\mu$. Appendix E contains results assuming inverted mass ordering. See section 2.3 for details.

bulk of them — which makes up their diffuse flux — remains unknown [6, 8, 14], although a handful of promising candidate sources have been identified [89–92]. In our analysis, we consider exclusively the diffuse neutrino flux, since only for it are measurements of the flavor composition available [25, 31–33]. These neutrinos are likely made in extragalactic cosmic-ray accelerators [8, 93–95]. Possible candidate source populations [93, 95] include active galactic nuclei [96], galaxy clusters [97–102], gamma-ray bursts [103–109], starburst galaxies [110–117], supernovae [118–120], and tidal disruption events [121–126], among others. In them, protons and other charged nuclei might be accelerated to energies of at least tens of PeV — and possibly much higher — within magnetized environments by means of collisionless shocks or other mechanisms [95].

Inside the sources, the high-energy protons interact with surrounding matter, in proton-proton (pp) collisions [127–129], or radiation, in proton-photon ($p\gamma$) collisions [128, 130–132]. These generate high-energy pions that, upon decaying, make neutrinos, i.e., $\pi^+ \rightarrow \mu^+ + \nu_\mu$, followed by $\mu^+ \rightarrow \bar{\nu}_\mu + e^+ + \nu_e$, and their charge-conjugated processes. (At higher energies, the decay of kaons and other production channels become important [130–134].) Each neutrino carries, on average, 5% of the energy of the parent proton [129, 130]. In production via pp collisions, the neutrino spectrum is a power law $\propto E^{-\gamma}$ that follows that of the parent protons, with the value of γ loosely expected to be in the interval [2,3]. In production via $p\gamma$ collisions, its shape depends on those of the parent protons and photons, and it is bump-like, on account of the photon spectrum peaking at a characteristic energy. Because the diffuse neutrino flux results from the addition of the emissions of all neutrino sources, the above features in the neutrino spectrum are softened. So far, IceCube observations are described well by an unbroken power with the value of γ dependent on the data set used and with little to no preference for alternative spectral shapes [7, 50], though this may change with further observations [135].

3.2 Neutrino detection and flavor composition

Presently, IceCube is the largest neutrino telescope [6, 136]: it consists of 1 km³ of deep Antarctic ice instrumented with photomultipliers. In it, high-energy neutrinos interact with nucleons in the ice, mainly via deep inelastic scattering [32, 137–139], either neutral-current (NC), i.e., $\nu_l + N \rightarrow \nu_l + X$, where $l = e, \mu, \tau$ and X are final-state hadrons, or charged-current (CC), i.e., $\nu_l + N \rightarrow l + X$. Final-state charged particles shower and emit Cherenkov radiation, which propagates through the ice and is detected by the photomultipliers. From the number of photons detected and from their spatial and temporal distributions, IceCube reconstructs the energy, direction, and flavor of the interacting neutrino [136, 140].

Broadly stated, IceCube detects three types of neutrino-induced events: tracks, cascades, and double cascades. Tracks are made mainly by CC interactions of ν_μ , where the final-state hadrons initiate a shower around the interaction vertex, and the final-state muon leaves a track of Cherenkov light in its wake, several kilometers in length and easily identifiable. Tracks are also made in 17% of ν_τ CC interactions where the final-state tauon decays into a muon [141]. Cascades are made by CC interactions of ν_e and ν_τ , where both the final-state lepton and hadrons shower around the interaction vertex, and by NC interactions of neutrinos of all flavors, where only the final-state hadrons shower. Double

cascades are made by CC interactions of ν_τ in which the final-state hadrons make a first shower, centered around the interaction vertex. The final-state tauon is energetic enough to decay some distance away, generating a second shower [33, 142, 143].

Starting events are those where the neutrino interacts within the detector volume. Because a large fraction of the neutrino energy is deposited in the ice, starting events trace neutrino energy closely [140]. A subset of them above 60 TeV are known as High-Energy Starting Events (HESE) [7]: they are subjected to a self-veto [144, 145] that reduces the contamination of atmospheric neutrinos and muons and, as a result, they have the highest content of neutrinos of astrophysical origin. However, its detection rate is relatively low, of approximately 10 events per year [7]. *Through-going tracks* are those where ν_μ (and ν_τ) interact outside the detector and produce muon tracks that cross part of it [50]. Their detection rate is orders-of-magnitude higher than for HESE, but, because they have lower energies, they are dominated by atmospheric neutrinos and muons, made in cosmic-ray interactions in the atmosphere. Further, for tracks, because the location of the neutrino interaction is unknown, the neutrino energy can only be inferred uncertainly [140]. In our analysis below, we exploit the combined capabilities of HESE and through-going events for flavor measurements, motivated by ref. [25].

Because different event types can be made by more than one neutrino flavor, a straightforward, event-by-event correspondence between detected event type and neutrino flavor is typically unfeasible, except for double cascades, which are only made by ν_τ . (In addition, showers made by the Glashow resonance [146], recently discovered by IceCube [147], are triggered exclusively by the interaction of 6.3-PeV $\bar{\nu}_e$ with electrons [148–151].) Still, from the relative number of detected events of different types, it is possible to infer statistically the flavor composition of the neutrino flux, i.e., the proportion of ν_e , ν_μ , and ν_τ in it, even if, because of the above limitations, the measurement uncertainties are significant. Our analysis below rests on the capabilities of IceCube and upcoming neutrino telescopes to infer the flavor composition in such a way, following the same spirit as refs. [42, 135, 152]

The flavor composition can be inferred either using only HESE showers, tracks, and double cascades, or by combining them with through-going muons. IceCube has reported the flavor composition in several analyses: using the first 3 years of HESE data [31], a combination of 4 years of contained events plus 2 years of through-going tracks [25], 5 years of contained events starting at lower energies [32], and, most recently, 7.5 years of HESE data, including a dedicated search for double cascades [33]. Independent analyses have reported complementary results; see, e.g., refs. [34–36, 153, 154]. The precision of these analyses is limited by the relative scarcity of HESE events. Presently, the most precise measurements come from the combined analysis of ref. [25], where the large number of through-going tracks pins down the flavor content of ν_μ . Such a combined analysis has not been updated since 2015 [25] in spite of the availability of larger event samples, on account of its complexity. Our analysis below is based on realistic estimates for what such analysis could look like with present and future data; see section 3.4.

3.3 Flavor composition of high-energy astrophysical neutrinos

Astrophysical sources emit high-energy ν_e , ν_μ , and ν_τ in the proportions $(f_{e,S}, f_{\mu,S}, f_{\tau,S})$, where $f_{\alpha,S} \leq 1$ ($\alpha = e, \mu, \tau$) is the ratio of $\nu_\alpha + \bar{\nu}_\alpha$ to the total emitted flux. We consider three benchmark scenarios of the flavor composition emitted by the sources often studied in the literature (see, e.g., refs. [37, 42, 155–162]): $(1/3, 2/3, 0)_S$, the canonical expectation from the full pion decay chain (see section 3.1); $(0, 1, 0)_S$, the muon-damped scenario where the intermediate muons created in pion decay cool by synchrotron radiation before decaying; and $(1, 0, 0)_S$, from the beta-decay of neutrons and isotopes. Below, we show the effect of the new matter potential in these three scenarios. Later, in section 4, we perform a full statistical analysis only for the full pion decay chain scenario.

For a given choice of flavor composition at the sources, en route to Earth neutrino oscillations modify it into

$$f_{\alpha,\oplus} = \sum_{\beta=e,\mu,\tau} \bar{P}_{\beta\alpha} f_{\beta,S}, \quad (3.1)$$

where the average oscillation probability, $\bar{P}_{\beta\alpha}$, is computed using eq. (2.19). During propagation, the total number of neutrinos is conserved; flavor transitions simply redistribute them into different flavors. Figure 5 shows the allowed regions of flavor composition at Earth under standard oscillations [42, 159], i.e., when the potential $V_{\alpha\beta} = 0$, for the three scenarios, and varying the values of the standard mixing parameters within their present-day 1σ allowed ranges [16, 17]. In the presence of long-range interactions, i.e., when $V_{\alpha\beta}$ is nonzero, because the flavor-transition probabilities are modified, so is the flavor composition at Earth. In this case, the flavor composition becomes energy-dependent, via the probability, in contrast to the flavor composition computed under standard oscillations.

Figure 5 illustrates the expected flavor composition at Earth in the presence of the new matter potential, under the $L_e - L_\mu$ and $L_\mu - L_\tau$ symmetries, for a representative neutrino energy of 100 TeV, and for the three benchmark scenarios of flavor composition at the sources. Results under the $L_e - L_\tau$ symmetry are similar to those under $L_e - L_\mu$; see figure 11. In figure 5, we compute $f_{\alpha,\oplus}$ for varying values of the long-range matter potential, $V_{\alpha\beta}$, and of the standard mixing parameters, within their 1σ allowed ranges [16, 17]. For small values of the potential, i.e., $V_{\alpha\beta} \lesssim \Delta m_{21}^2 / (2E) \sim 10^{-20}$ eV, the flavor composition is close to the expectation from standard oscillations. As the potential grows, the behavior of the flavor composition traces that of the flavor-transition probabilities (figures 4 and 10): the wiggles in $f_{\alpha,\oplus}$ reflect the resonant features in the probabilities. For large values of the potential, i.e., $V_{\alpha\beta} \gtrsim 10^{-16}$ eV, the new matter potential becomes the dominant contribution to the Hamiltonian, eq. (2.14). In that case, because the contribution of the new potential is flavor-diagonal, flavor transitions are suppressed (section 2.3). Accordingly, figure 5 shows that the flavor composition at Earth is the same as at the sources, i.e., $f_{\alpha,\oplus} \approx f_{\alpha,S}$.

3.4 Analysis choices

Flavor composition at the sources independent of energy. Because different neutrino production channels become available at different energies [129, 130, 132, 134], the

flavor composition emitted by the sources, $f_{\alpha,S}$, may vary with energy [156, 157, 159, 163–165], contingent on key source properties like the magnetic field intensity [166, 167]. Nevertheless, adopting the same practice as IceCube flavor measurements [25, 31–33], we take $f_{\alpha,S}$ to be constant within the energy range of our analysis. This is justified by the limited number of HESE events, which would be further diluted by attempting to measure the flavor composition in multiple energy bins. Under this assumption, any energy dependence that the flavor composition at the Earth, $f_{\alpha,\oplus}$, might have is due solely to the presence of the new neutrino-matter interaction. Reference [158] explores the interplay between energy dependence that stems from neutrino production and from new physics.

Averaging $f_{\alpha,\oplus}$ between ν and $\bar{\nu}$. Because, in high-energy neutrino telescopes, events triggered by neutrinos and antineutrinos are so far indistinguishable from one another, we average the flavor composition at Earth between neutrinos and antineutrinos, assuming they are present in equal proportions in the flux that reaches Earth. In actuality, their proportions are practically unknown (see, however, refs. [147, 168]), but the above assumption aligns with theoretical expectations, especially from multi-pion neutrino production at high energies; see, e.g., ref. [132]. As a result of averaging, the resonant features in the oscillation probabilities, which are more prominent for neutrinos than for antineutrinos (figure 4), appear softened in the flavor composition at Earth that we use.

Averaging $f_{\alpha,\oplus}$ over energy. In figures 4 and 5, we illustrated the effect of the new matter potential on the flavor-transition probabilities and flavor ratios for a fixed neutrino energy of 100 TeV. However, IceCube detects neutrinos with different energies in the range TeV–PeV. Within it, the spectrum of ν_α is described well by a power law $\Phi_\alpha(E) \propto f_{\alpha,\oplus}(E)E^{-\gamma}$, where the value of the spectral index is $\gamma \in [2, 3]$. To produce our results, we fix $\gamma = 2.5$ [25]. As in ref. [26], we account for the neutrino energy distribution by averaging the flux within the energy range of 25 TeV–2.8 PeV [25], i.e., $\langle \phi_\alpha \rangle \approx (2.8 \text{ PeV})^{-1} \int dE \phi_\alpha(E)$. Below, to produce our results, we use the energy-averaged flavor ratios computed from the average fluxes, i.e., $\langle f_{\alpha,\oplus} \rangle \approx \langle \phi_\alpha \rangle / \sum_\beta \langle \phi_\beta \rangle$.

Estimates of present and future flavor sensitivity. In our analysis, we use estimates of the present-day flavor sensitivity of IceCube and of future detectors; see figure 5. These are based on estimated combined analyses of HESE events plus through-going tracks (see section 3.2), motivated by ref. [25], which offer the greatest sensitivity. We adopt the flavor measurement projections for IceCube-Gen2 from ref. [15], which were generated assuming a plausible neutrino spectrum $\propto E^{-2.5}$. Because these projections were only generated assuming a flavor composition at the sources of $(1/3, 2/3, 0)_S$, later we only derive constraints on long-range neutrino interactions for that one benchmark scenario. As in ref. [42], we isolate the contributions of IceCube and IceCube-Gen2 to the flavor sensitivity from ref. [15]. This allows us to generate results based on estimates of the present-day flavor sensitivity, for the year 2020, using 8 years of IceCube, and forecasts for the year 2040, using 15 years of IceCube plus 10 years of IceCube-Gen2, and using the additional contribution of future neutrino telescopes Baikal-GVD [43], KM3NeT [44], P-ONE [45], and TAMBO [46]. Following ref. [42], we assume that future detectors will have

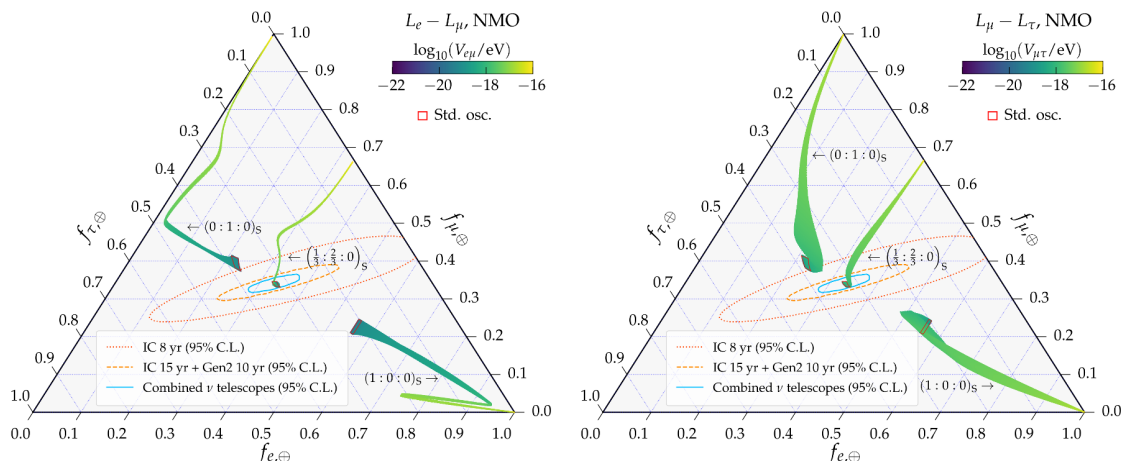


Figure 5. Flavor composition of high-energy astrophysical neutrinos at Earth, $f_{\alpha,\oplus}$, as a function of the long-range matter potential $V_{e\mu}$, under $L_e - L_\mu$ (left), or $V_{\mu\tau}$, under $L_\mu - L_\tau$ (right). We show results for three benchmark choices of the flavor composition at the sources, $(f_{e,S}, f_{\mu,S}, f_{\tau,S}) = (1/3, 2/3, 0)$, the canonical expectation, $(0, 1, 0)$, and $(1, 0, 0)$, compared to the expectation from standard oscillations (“Std. osc.”). The flavor composition is averaged between neutrinos and antineutrinos, assuming they exist in equal proportion in the flux. For this plot only, we fix the neutrino energy to 100 TeV, assume normal neutrino mass ordering, and vary the standard mixing parameters within their 1σ allowed ranges; our statistical methods systematically vary these choices. Flavor-composition predictions are compared against three estimates of the flavor sensitivity of neutrino telescopes using 8 years of IceCube data (“IC 8 yr”), 15 years of IceCube data plus 10 years of IceCube-Gen2 (“IC 15 yr + Gen2 10 yr”), and the combined exposure of all neutrino telescopes available by 2040 (“Combined ν telescopes”). For $L_e - L_\tau$, results are similar as for $L_e - L_\mu$; see appendix D. See section 3.3 for details.

the same detection efficiency of HESE and through-going tracks as IceCube (see section 4), though with different rates, and rescale the IceCube flavor sensitivity to their respective expected exposures. This is admittedly a simplification, made necessary by the current absence of details on the capabilities of future detectors.

4 Statistical analysis and results

Our goal is to compute the bounds on the long-range-interaction parameters — the mediator mass, $m'_{\alpha\beta}$, and the coupling, $g'_{\alpha\beta}$ — that can be placed by measuring the flavor composition. To do this, we contrast our predictions of the flavor composition obtained under long-range interactions (section 3.3) against the estimated present and future flavor-measuring capabilities of IceCube and other upcoming detectors (section 3.4). First, we compute bounds on the long-range matter potential, $V_{\alpha\beta}$; then, we translate them into bounds on the mediator mass and coupling.

4.1 Statistical analysis

We adopt the Bayesian statistical methods introduced in ref. [42]. For given flavor ratios at the source, $f_{\alpha,S}$, we assume one of the three benchmark scenarios outlined in section 3.3.

Observation epoch	Neutrino telescopes	Neutrino mixing parameters
2020 (estimated)	IC 8 yr	NuFit 5.1 (2021)
2040 (projected)	IC 15 yr + IC-Gen2 10 yr	NuFit 5.1 + JUNO + DUNE + HK
2040 (projected)	Combined ν telescopes	NuFit 5.1 + JUNO + DUNE + HK

Table 1. *Observation epochs of our analysis: years 2020 and 2040.* For each epoch, we show the neutrino telescopes that measure the flavor composition of high-energy astrophysical neutrinos and the oscillation experiments that constrain the value of the neutrino mixing parameters. We assume that upcoming neutrinos have flavor-measuring capabilities similar to those of IceCube. In 2040, the combined telescopes include IceCube, IceCube-Gen2 [15], Baikal-GVD [43], KM3NeT [44], P-ONE [45], and TAMBO [46]. See section 3.2 for details. For our 2040 projections of the measurement of mixing parameters, we assume that their real values are the present-day best-fit values from the NuFit 5.1 global oscillation fit [16, 17]. See section 2.3 for details.

Then, for test values of the long-range potential, $V_{\alpha\beta}$, and of the mixing parameters, $\boldsymbol{\vartheta} \equiv (s_{12}^2, s_{23}^2, s_{13}^2, \delta_{\text{CP}})$, with $s_{ij} \equiv \sin^2 \theta_{ij}$, we compute the associated energy-averaged flavor composition at Earth, $\langle \mathbf{f}_{\oplus} \rangle \equiv (\langle f_{e,\oplus} \rangle, \langle f_{\mu,\oplus} \rangle, \langle f_{\tau,\oplus} \rangle)$, using the procedure introduced in section 3.4. We assess the compatibility of these predictions with measurements of the flavor composition in neutrino telescopes through three factors: $\pi(V_{\alpha\beta})$, the prior associated to the value of $V_{\alpha\beta}$; $\pi(\boldsymbol{\vartheta})$, the prior associated to the value of $\boldsymbol{\vartheta}$; and $\mathcal{L}(\langle \mathbf{f}_{\oplus} \rangle)$, the likelihood of having measured the flavor composition $\langle \mathbf{f}_{\oplus} \rangle$. We expand on these factors below. Using them, we compute the posterior probability density of $V_{\alpha\beta}$, marginalized over all possible values of the mixing parameters, i.e.,

$$\mathcal{P}(V_{\alpha\beta}) = \int d\boldsymbol{\vartheta} \mathcal{L}(\langle \mathbf{f}_{\oplus}(V_{\alpha\beta}, \boldsymbol{\vartheta}) \rangle) \pi(\boldsymbol{\vartheta}) \pi(V_{\alpha\beta}) . \quad (4.1)$$

This method represents an improvement over the one used in the original study of long-range interactions using the flavor composition, ref. [26]. There, the sensitivity to long-range interactions was derived from a straightforward comparison of the predicted flavor composition vs. the flavor sensitivity of IceCube, and the method was not amenable to being generalized to compute sensitivity beyond the 1σ statistical significance. Here, in contrast, the Bayesian approach allows us to derive limits at higher statistical significance and to properly account for the prior on mixing parameters.

Table 1 summarizes the two epochs for which we perform the above analysis: the present, represented by the year 2020, and the future, represented by the year 2040. Each epoch has an associated precision on mixing parameters and flavor measurements associated to it, encoded in the prior $\pi(\boldsymbol{\vartheta})$ and the likelihood $\mathcal{L}(\langle \mathbf{f}_{\oplus} \rangle)$. We expand on them below.

Prior on the long-range matter potential, $\pi(V_{\alpha\beta})$. To avoid introducing unnecessary bias, we use a uniform prior on $V_{\alpha\beta}$ in the interval 10^{-24} – 10^{-16} eV. This interval covers the full range of long-range-interaction effects: towards the lower end, standard oscillations dominate, and towards the upper end, long-range interactions dominate.

Prior on the mixing parameters, $\pi(\boldsymbol{\vartheta})$. We take the prior of each mixing parameter, today and in the future, to be centered at its present-day best-fit value from the

NuFit 5.1 [16, 17] global oscillation fit. The distributions for s_{12}^2 and s_{13}^2 are each normal and uncorrelated with other parameters, while those of s_{23}^2 and δ_{CP} are correlated. For our 2020 estimates, we use the NuFit 5.1 χ^2 distributions to compute the joint likelihood, $-2 \ln \mathcal{L}_{2020} \equiv \chi^2(s_{12}^2) + \chi^2(s_{13}^2) + \chi^2(s_{23}^2, \delta_{\text{CP}})$. For our 2040 projections, we combine this with future measurements of θ_{12} by JUNO, as computed in ref. [42], and of θ_{23} and δ_{CP} by DUNE [47] and HK [48], which we generate ourselves. We do so in dedicated simulations using GLOBES [169], and adopting the detector descriptions for DUNE [170, 171], using 3.5 years of runtime in neutrino and antineutrino modes each (using a revised plan of 5 years for each would not change results significantly [172]), and for HK [48], using 2.5 years of runtime in neutrino mode and 7.5 years in antineutrino mode. (For θ_{23} and δ_{CP} , our projections differ from those of ref. [42] because we generate them using the best-fit values from NuFit 5.1 [16, 17] instead of NuFit 5.0, as a result of which the value of θ_{23} has shifted from the upper octant to the lower octant [173].) For s_{13}^2 , we keep the width of its prior fixed to its present-day size, which is dominated by measurements in Daya Bay [174], as they are not expected to be improved upon significantly by 2040. In summary, for 2040, we use the likelihood $-2 \ln \mathcal{L}_{2040} \equiv -2 \ln \mathcal{L}_{2020} + \sum_{\mathcal{E}} \chi_{\mathcal{E}}^2$, where the contribution of DUNE, HK, and JUNO is each $\chi_{\mathcal{E}}^2 = \sum_{i,j} (\vartheta_i - \bar{\vartheta}_i) \Sigma_{\mathcal{E},ij}^{-1} (\vartheta_j - \bar{\vartheta}_j)$, Σ_{ij} is the covariance matrix for the mixing parameters ϑ_i , ϑ_j , and $\bar{\vartheta}_i$, $\bar{\vartheta}_j$ are their assumed real values.

Likelihood of flavor measurement, $\mathcal{L}(\langle \mathbf{f}_{\oplus} \rangle)$. The likelihood of flavor measurement represents the precision with which neutrino telescopes can measure the flavor composition. For the 2020 and 2040 epochs, we adopt the same flavor likelihoods as ref. [42]. By construction, they are centered on the canonical flavor composition at Earth, near $(1/3, 1/3, 1/3)_{\oplus}$, that is expected from neutrino production via the full pion decay chain (section 3.1). Hence, the bounds on long-range interactions that we derive later are obtained under the assumption that the true value of the measured flavor is such. For our 2020 estimates, we adopt an estimate of the IceCube flavor sensitivity that would be obtained using 8 years of HESE events and through-going tracks [15], assuming a flux with spectral index $\gamma = 2.5$. For our 2040 projections, we adopt either the expected flavor sensitivity from 15 years of IceCube plus 10 years of IceCube-Gen2 measurements, extracted from ref. [15], or the combined sensitivity from that plus the expected 2040 sensitivity of Baikal-GVD [43], KM3NeT [44], P-ONE [45], and TAMBO [46], extracted from ref. [42], which we defer to for details. As illustration, figure 5 shows 95% C.L. contours for the 2020 and 2040 flavor-measurement likelihoods.

4.2 Results

Figure 6 shows the resulting posteriors of $V_{e\mu}$, under the $L_e - L_{\mu}$ symmetry, and of $V_{\mu\tau}$, under the $L_{\mu} - L_{\tau}$ symmetry, computed using eq. (4.1), for the years 2020 and 2040. Results for $V_{e\tau}$, under the $L_e - L_{\tau}$ symmetry, are similar to $V_{e\mu}$; see appendix D. The posteriors are maximum at a potential of roughly 10^{-19} eV. Because the posteriors plateau at lower values, we can place upper limits on the values of the potentials. Values above roughly 10^{-18} eV are noticeably less favored, and they become more so when moving from

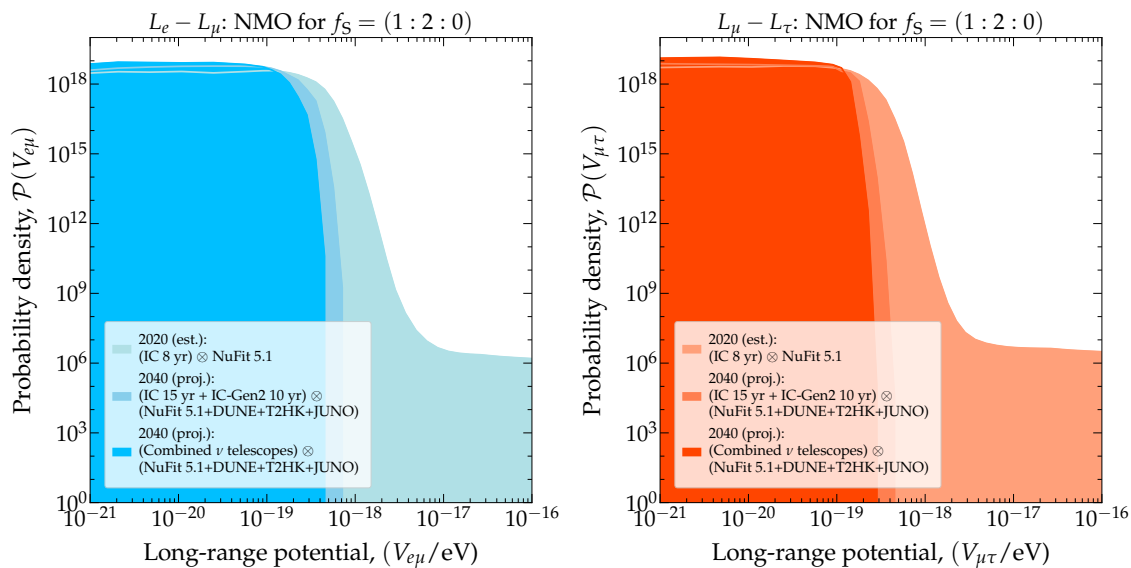


Figure 6. Posterior probability density of the long-range matter potentials $V_{e\mu}$, under the $L_e - L_\mu$ symmetry (left) and $V_{\mu\tau}$, under the $L_\mu - L_\tau$ symmetry (right). We assume a measurement of the flavor composition at Earth centered around the canonical expectation of about $(1/3 : 1/3 : 1/3)_\oplus$, corresponding to $f_S = (1/3 : 2/3 : 0)$ at the sources; see figure 5. See figure 7 for the limits on the potential derived from the posterior. Results for $V_{e\tau}$, under the $L_e - L_\tau$ symmetry, are similar to $V_{e\mu}$; see appendix D. We assume that all neutrino telescopes available by 2040 have detection efficiencies similar to that of IceCube (section 3.4). Results here are obtained assuming normal neutrino mass ordering (NMO); results for inverted ordering are in appendix E. See section 4.1 for details.

2020 to 2040 due to improvements in the precision of the mixing parameters and flavor composition, i.e., to narrower $\pi(\boldsymbol{\vartheta})$ and $\mathcal{L}(\boldsymbol{f}_\oplus)$, respectively.

Figure 7 (also table 2) shows the resulting upper limits on the long-range potentials. A limit has value of $V_{\alpha\beta}^*$ such that the integral of the posterior, $\int_0^{V_{\alpha\beta}^*} \mathcal{P}(V_{\alpha\beta}) dV_{\alpha\beta}$, equals a desired credible level (C.L.). We show limits at the 95% C.L in figure 7 (also in figures 1, 8, and 12). Differences in the limits obtained under different symmetries are moderate because, under the assumption of $(1/3, 2/3, 0)_S$, their predicted flavor compositions at Earth are only moderately different; see figures 5 and 11.

Figure 7 reveals modest improvement in the limits between 2020 and 2040, of a factor of 2.5–3, and marginal improvement in 2040 between using only IceCube plus IceCube-Gen2 and using all future available telescopes. Given the significant increase in the combined neutrino detection rate between 2020 and 2040 (see figure 1 in ref. [42]), and between using only IceCube plus IceCube-Gen2 and all telescopes, this is unexpected at first glance. Yet, close inspection of the variation of the flavor composition at Earth with the long-range potential in figure 5 reveals the subtle reason. For the canonical choice of flavor composition at the sources of $(1/3, 2/3, 0)_S$, which we have adopted to obtain the limits on the long-range potential, the flavor composition at Earth approaches the center of the flavor triangle — where the likelihood of flavor measurement is largest and from whence

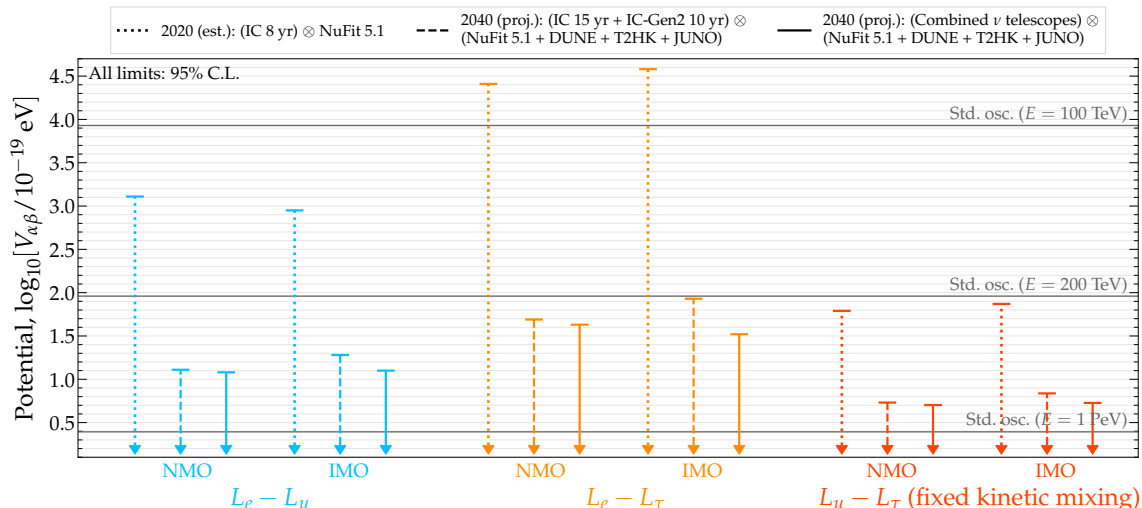


Figure 7. Upper limits (95% C.L.) on the long-range potential induced by the $L_e - L_\mu$, $L_e - L_\tau$, and $L_\mu - L_\tau$ symmetries, estimated for 2020 and projected for 2040. For comparison, we show the standard-oscillation contribution (“Std. osc.”) to the Hamiltonian, $\Delta m_{21}^2/(2E)$, evaluated at the present-day best-fit value of Δm_{21}^2 [16, 17] and at different values of the neutrino energy, E . We assume that all neutrino telescopes available by 2040 have detection efficiencies similar to that of IceCube (section 3.4). Figure 8 shows these limits translated into limits on the coupling, $g'_{\alpha\beta}$. See appendix F for the values of the limits. See section 4 for details.

the limit is predominantly derived — from the direction along which the gradients of the 2020 and 2040 likelihoods resemble each other the most.

Figure 8 shows how the upper limits on the potential translate into upper limits on the coupling, $g'_{\alpha\beta}$, as a function of the mediator mass, $m'_{\alpha\beta}$. In figure 8, each limit is an isocontour of potential in the $g'_{\alpha\beta}-m'_{\alpha\beta}$ plane; we use eq. (2.7) to translate the limits on $V_{\alpha\beta}$ in figure 7 into the limits in figure 8. Thus, the step-like transitions in figure 8 have the same origin as those of the potential itself (figure 3): the limits on $g'_{\alpha\beta}$ are stronger for smaller mediator masses, where the potential is due to a larger number of electrons or neutrons. Figure 1 spotlights our 2020 projections combining all neutrino telescopes.

For $L_e - L_\mu$ (and also for $L_e - L_\tau$, see appendix D), figure 8 reveals that already our 2020 estimate is better, by about one order of magnitude, than the proof-of-principle sensitivity based on 2015 IceCube flavor measurements from ref. [26]. (However, a fair comparison is not possible due to differences in their statistical significance and methods.). For $L_\mu - L_\tau$, we estimate and forecast limits based on the flavor composition for the first time. The limits for $g'_{\mu\tau}$ shown in figure 8 were obtained by fixing the mixing strength to $(\xi - \sin \theta_W \chi) = 5 \times 10^{-24}$ (see section 2.1). Because $V_{\mu\tau} \propto g'_{\mu\tau}(\xi - \sin \theta_W \chi)$ (see eqs. (2.5) and (2.6)), given an upper limit on $V_{\mu\tau}$, a smaller value of the mixing strength, which is plausible, would entail a weaker limit on $g'_{\mu\tau}$. (Alternatively, the limits for $L_\mu - L_\tau$ in figure 8 can be interpreted as being on the product of the coupling times the mixing strength, without any assumption on the value of the latter.)

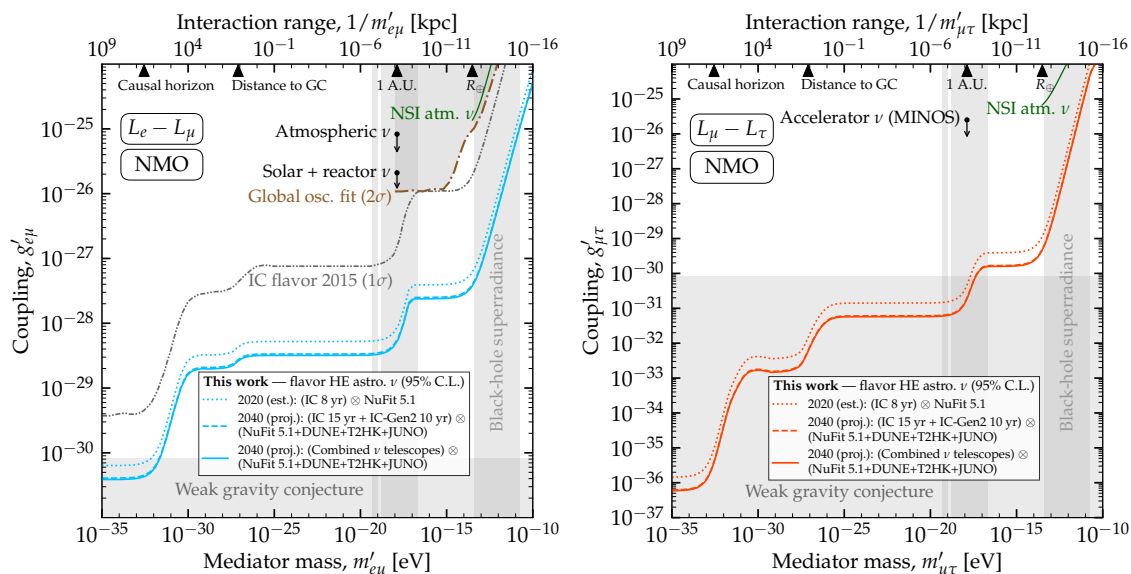


Figure 8. Estimated present-day (2020) and projected (2040) upper limits (95% C.L.) on the coupling strength, $g'_{\alpha\beta}$, of the new boson, $Z'_{\alpha\beta}$, with mass $m'_{\alpha\beta}$, that mediates flavor-dependent long-range neutrino interactions. Same as figure 1, but now showing also the projected 2040 limits using either IceCube plus IceCube-Gen2, or those combined with Baikal-GVD, KM3NeT, P-ONE, and TAMBO. *Left:* limits on neutrino-electron interactions under the $L_e - L_\mu$ gauge symmetry. *Right:* limits on neutrino-neutron interactions under the $L_\mu - L_\tau$ gauge symmetry; existing limits from accelerator neutrinos in MINOS (95% C.L.) are from ref. [18]. See section 4 for details.

Figure 8, and also figures 1 and 12, show that, for $L_e - L_\mu$ and $L_e - L_\tau$, our limits, both estimated for 2020 and forecast for 2040, improve on existing ones obtained from atmospheric neutrinos [20], solar and reactor neutrinos [21], reinterpretations [27] of bounds on the coefficients of non-standard neutrino interactions (NSI) [19, 22–24] (see appendix C), and the recent global oscillation fit from ref. [19]. For $L_\mu - L_\tau$, light mediators in the mass range that we consider are largely unconstrained, except towards high masses, from accelerator neutrinos [18] and NSI.

In summary, our results show that, already today, the estimated flavor sensitivity of IceCube and the uncertainty in the mixing parameters have the potential to significantly improve the constraints on flavor-dependent long-range neutrino interactions.

5 Future improvements

The goal of our analysis is to estimate the reach of flavor composition of high-energy astrophysical neutrinos to constrain flavor-dependent long-range neutrino interactions rather than providing detailed results based on real flavor measurements. In doing so, we incorporated assumptions in our analysis towards facilitating our estimates. Below, we list them and point out with envisioned improvements.

Alternative flavor composition choices. To produce our limits, we limited ourselves only to the case where the flavor composition at Earth is the canonical expectation

of $(1/3, 1/3, 1/3)_{\oplus}$, from neutrino production via the full pion decay production, $(1/3, 2/3, 0)_{\text{S}}$. This was due to the unavailability of the projected flavor sensitivity of neutrino telescopes to alternative choices of flavor composition (section 3.4), but our methods are general and applicable also in those alternatives. We encourage experimental collaborations to make publicly available the flavor sensitivity of their experiments under assumptions other than the canonical one.

Flavor-measurement capabilities of upcoming detectors. Our forecasts for upcoming neutrino telescopes — Baikal-GVD, IceCube-Gen2, KM3NeT, P-ONE, TAMBO — assume that their capabilities to measure the flavor composition will be similar to those of IceCube. This is a necessary assumption given the absence of their realistic capabilities at the time of writing. However, it is foreseeable already that differences in their geometries — most notably, in the spacing between photomultiplier strings — will imply differences between their detection capabilities. Further, we have not considered the possibility of proposed improvements in flavor-tagging techniques, like those provided by muon and neutron echoes [175]. As the specific flavor-measurement capabilities of different upcoming experiments become better defined, future versions of our analysis will be able to incorporate them.

Using the energy dependence of the flavor composition. Our results are based on the comparison of the energy-averaged flavor composition at Earth vs. the flavor composition measured over an energy interval, assuming that it is constant within it (section 3.4). However, long-range interactions modify the flavor composition in an energy-dependent way, so there may be additional probing power to be reaped from measuring the flavor composition in multiple energy bins. Present-day event rates are likely insufficient to do this, but IceCube-Gen2 may be able to [15]. Further, doing this could allow us to distinguish between the variation of the flavor composition with energy that stems from long-range interactions from the one that stems from the neutrino production mechanism changing with energy, e.g., from full pion decay chain at low energies to muon-damped at high energies [157–159, 163–167].

Astrophysical uncertainties. To produce our results, we assumed that the energy spectrum of the high-energy astrophysical neutrinos is a power law $\propto E^{-\gamma}$, with fixed $\gamma = 2.5$, compatible with IceCube analyses that combine HESE events and through-going tracks [25]. However, the value of γ is only uncertainly known and varies somewhat depending on the data set used to measure it [7, 50]. Further, the IceCube observations admit a description with differently shaped energy spectra; e.g., refs. [7, 50, 117, 135, 176, 177]. Finally, because the diffuse flux of neutrinos is the addition of contributions from sources located at different distances, it depends on how the number density of sources evolves with redshift, which we have neglected in our analysis. Incorporating uncertainties in the shape of the neutrino spectrum and the redshift distribution of sources would likely weaken the bounds that we report, though a full analysis is beyond the scope of this paper.

Computing neutrino propagation. When computing the long-range matter potential (section 2.2), we do so at the location where the neutrinos are detected, at IceCube, rather than propagating neutrinos from their astrophysical sources to Earth and computing the changing potential at every point along their trajectory. This simplified treatment allows us to first put limits on the long-range potential and then to translate those into limits on $g'_{\alpha\beta}$. Our method overestimates the influence of faraway electrons and neutrons, but mainly for limits at large mediator masses. Reference [19] is an example of how to compute long-range interactions during propagation, though only for neutrino propagation inside the Earth and the Sun.

Screening due to relic neutrinos. If the background of relic neutrinos contains ν_e and $\bar{\nu}_e$ in equal proportions, it may partially screen the long-range potential due to cosmological electrons [20, 178, 179]. The Debye length [20], i.e., the distance at which the screening becomes important, is a factor-of-10 shorter than the long-range interaction range, so screening would affect limits at mediator masses below about 10^{-30} eV.

6 Summary and outlook

Neutrinos may conceivably undergo interactions with matter beyond those contained in the Standard Model. If so, they must necessarily be weak up to neutrino energies of a few hundred GeV in order to have gone undetected so far. Yet, at higher energies, accessible via recently detected astrophysical neutrinos, they may be significant or even prominent. If discovered, they would represent compelling evidence of new physics.

We have studied the sensitivity to new flavor-dependent interactions between neutrinos and electrons and neutrinos and neutrons, today and in the future. They result from gauging the lepton-number symmetries $L_e - L_\mu$, $L_e - L_\tau$, or $L_\mu - L_\tau$ that are already global symmetries of the Standard Model. The interaction is mediated by a new neutral gauge boson that, if ultra-light (i.e., lighter than 10^{-10} eV), subtends a prodigious interaction range, from km to Gpc. As a result, neutrinos may be affected by the aggregated matter potential sourced by large collections of nearby and faraway matter — the Earth, Moon, Sun, Milky Way, and the cosmological distribution of matter. The interactions may modify neutrino oscillations, especially at high energies, and, if significant, may suppress them.

Thus, we have estimated and forecast constraints on long-range interactions using the highest-energy neutrinos known: the TeV–PeV astrophysical neutrinos discovered by IceCube [1–8]. We employ the flavor composition of their diffuse flux, i.e., the proportion of ν_e , ν_μ , and ν_τ in it: since the flavor composition reflects the effect of neutrino oscillations en route to Earth, it may reveal the presence of flavor-dependent long-range interactions.

We combine the estimated flavor-measuring capabilities of IceCube with present-day uncertainties on the standard neutrino mixing parameters that drive neutrino oscillations [16, 17]. Our work improves and extends ref. [26], chiefly by adopting superior statistical methods, and by considering the $L_\mu - L_\tau$ symmetry. Our analysis choices are conservative and realistic (section 3.4). Because we rely on estimates of the flavor sensitivity, our goal is to showcase the capacity of neutrino telescopes, rather than provide high-precision results, and to motivate further work.

Presently, there is large uncertainty in the measurement of the flavor composition at IceCube and moderate-to-large uncertainties on the neutrino mixing parameters. At first glance, this should reduce sensitivity to long-range interactions. Surprisingly, we find that *using the estimated current flavor sensitivity of IceCube and current mixing parameter uncertainties, high-energy astrophysical neutrinos could tightly constrain long-range interactions, surpassing existing limits (see figure 1).*

In the coming two decades, the above limitations will likely be overcome by next-generation neutrino oscillation experiments — DUNE [47], Hyper-Kamiokande [48], and JUNO [49] — and by high-energy neutrino telescopes — IceCube-Gen2 [15], Baikal-GVD [43], KM3NeT [44], P-ONE [45], and TAMBO [46]. By 2040, nominally, we anticipate modest improvements from repeating our analysis unchanged but possible substantial gains by upgrading it to leverage higher event rates and potential advancements in flavor composition measurement (section 5).

The discovery of a new fundamental interaction would mark groundbreaking progress. Our findings show that high-energy astrophysical neutrinos, already today, have the potential to probe this more rigorously than present-day constraints.

Acknowledgments

We thank Pilar Coloma, Francis Halzen, Masoom Singh, and Yu-Dai Tsai for their helpful discussions and crucial inputs. S.K.A., S.D., and A.N. acknowledge the support from the Department of Atomic Energy (DAE), Govt. of India, under the Project Identification no. RIO 4001. S.K.A. is supported by the Young Scientist Project [INSA/SP/YSP/144/2017/1578] from the Indian National Science Academy (INSA). S.K.A. acknowledges the financial support from the Swarnajayanti Fellowship (sanction order no. DST/SJF/PSA-05/2019-20) provided by the Department of Science and Technology (DST), Govt. of India. S.K.A. and A.N. receive the financial support from the Research Grant (sanction order no. SB/SJF/2020-21/21) provided by the Science and Engineering Research Board (SERB), Govt. of India, under the Swarnajayanti Fellowship project. S.K.A. would like to thank the United States-India Educational Foundation (USIEF) for providing the financial support through the Fulbright-Nehru Academic and Professional Excellence Fellowship (Award no. 2710/F-N APE/2021). M.B. is supported by the VILLUM FONDEN under project no. 29388. The numerical simulations are carried out using the “SAMKHYA: High-Performance Computing Facility” at the Institute of Physics, Bhubaneswar, India.

A Interaction potential under the $L_\mu - L_\tau$ symmetry

Under the $L_e - L_\mu$ and $L_e - L_\tau$ symmetries, neutrinos couple directly to electrons via $Z'_{e\beta}$ ($\beta = \mu, \tau$), i.e., via the term $\mathcal{L}_{Z'}$ of the Lagrangian, eq. (2.3) in the main text; see figure 2. Under the $L_\mu - L_\tau$ symmetry, such direct interaction does not occur due to the absence of naturally occurring muons and tauons. But, after breaking the $L_\mu - L_\tau$ symmetry, there are terms in the interaction Lagrangian that mix the field strength tensors and the two massive bosons, Z and $Z'_{\mu\tau}$, which facilitate neutrino interactions with matter; see figure 2.

For ordinary, electrically neutral matter, this interaction is

$$\mathcal{L}_{\text{int}} = -g'(\xi - \sin\theta_W\chi)\frac{e}{\sin\theta_W\cos\theta_W}J'_\rho J_3^\rho, \quad (\text{A.1})$$

where $J'_\rho = \bar{\nu}_\mu\gamma_\rho P_L\nu_\mu - \bar{\nu}_\tau\gamma_\rho P_L\nu_\tau$, $J_3^\rho = -\frac{1}{2}\bar{e}\gamma^\rho P_L e + \frac{1}{2}\bar{u}\gamma^\rho P_L u - \frac{1}{2}\bar{d}\gamma^\rho P_L d$, and the term $(\xi - \sin\theta_W\chi)$ accounts for Z - Z' mixing (figure 2).

The time component of J_3^ρ , relevant for static matter, is

$$J_3^0 = -\frac{1}{4}\left[\bar{e}\gamma^0(1-\gamma^5)e - \bar{u}\gamma^0(1-\gamma^5)u + \bar{d}\gamma^0(1-\gamma^5)d\right], \quad (\text{A.2})$$

which, for an unpolarized medium, becomes

$$J_3^0 = -\frac{1}{4}(n_e - n_u + n_d) = -\frac{1}{4}(n_e - n_p + n_n), \quad (\text{A.3})$$

where n_f ($f = e, u, d$) is the number density of electrons, up quarks, and down quarks. For electrically neutral medium, $n_p = n_e$, so, $J_3^0 = -n_n/4$. Replacing this in eq. (A.1) yields the potential due to neutrons under the $L_\mu - L_\tau$ symmetry,

$$V_{\mu\tau} = g'_{\mu\tau}(\xi - \sin\theta_W\chi)\frac{e}{4\sin\theta_W\cos\theta_W}n_n. \quad (\text{A.4})$$

B Evolution of the modified mixing angles with long-range potential

Figure 9 shows the evolution of the modified mixing angles with the long-range potential. In the main text, the average oscillation probability, eq. (2.19), depends on the unitarity matrix \mathbf{U}^m that diagonalizes the Hamiltonian, eq. (2.14), which includes contribution from the long-range matter potential. The matrix \mathbf{U}^m is parametrized as the PMNS matrix, but in terms of three new mixing angles, θ_{12}^m , θ_{23}^m and θ_{13}^m , and one CP-violating phase, δ_{CP}^m , that depend on the long-range potential. Reference [180] showed analytically that δ^m remains unchanged from its vacuum value, δ_{CP} .

C Reinterpretation of Super-Kamiokande NSI limits

Using the atmospheric neutrino data, the Super-Kamiokande experiment obtained bounds on the neutrino non-standard interaction (NSI) parameters involving only down quarks in the medium, i.e., $|\varepsilon_{\mu\mu}^d - \varepsilon_{\tau\tau}^d| < 0.049$ at 90% C.L. [22]. In our convention, we consider the NSIs due to electrons in the medium, i.e., $|\varepsilon_{\mu\mu} - \varepsilon_{\tau\tau}| = 3 \times |\varepsilon_{\mu\mu}^d - \varepsilon_{\tau\tau}^d| < 0.147$, since $N_d \approx 3N_e$ inside the Earth. Reference [27] reinterpreted these bounds on the NSI parameters as limits on long-range neutrino interactions under the $L_e - L_\mu$ and $L_e - L_\tau$ symmetries. Below, we revisit explicitly these limits and extend them to the $L_\mu - L_\tau$ symmetry. We obtain limits on the potentials $V_{e\mu}$, $V_{e\tau}$, and $V_{\mu\tau}$; in figures 1, 8, 12, and 17, we show them translated into limits on the coupling strength, via the definition of the potential, eq. (2.7).

The NSI matter potential is

$$\mathbf{V}_{\text{NSI}} = V_{\text{CC}} \begin{pmatrix} \varepsilon_{ee} & \varepsilon_{e\mu} & \varepsilon_{e\tau} \\ \varepsilon_{e\mu}^* & \varepsilon_{\mu\mu} & \varepsilon_{\mu\tau} \\ \varepsilon_{e\tau}^* & \varepsilon_{\mu\tau}^* & \varepsilon_{\tau\tau} \end{pmatrix}, \quad (\text{C.1})$$

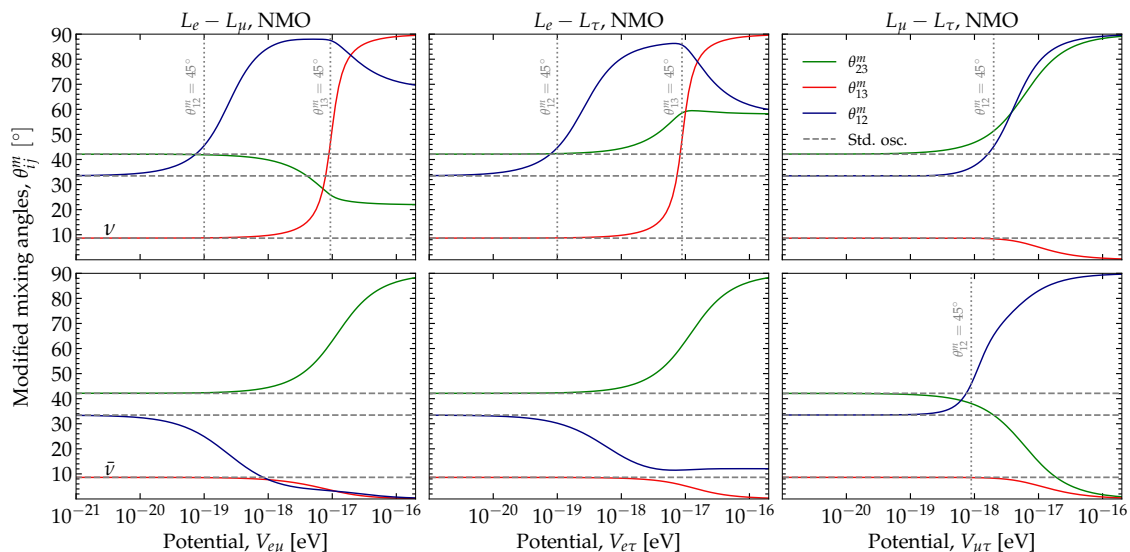


Figure 9. Modified mixing angles as functions of the long-range matter potential induced by the $U(1)$ gauge symmetries $L_e - L_\mu$ (left column), $L_e - L_\tau$ (middle column), and $L_\mu - L_\tau$ (right column). Results are for neutrinos and antineutrinos at a fixed energy of 100 TeV, assuming normal mass ordering (NMO). Vertical lines mark the values of the potential for which θ_{12}^m and θ_{13}^m become resonant. Values of the mixing angles under standard oscillations (“Std. osc.”), i.e., for $V_{\alpha\beta} = 0$, are shown for comparison. The standard mixing parameters are fixed at their present-day best-fit values from NuFit 5.1 [16, 17]. See section 2.3 for details.

where V_{CC} is the charged-current SM potential from electrons, as defined for eq. (2.17) in the main text. The parameters $\varepsilon_{\alpha\beta}$ represent the strength of NSI between neutrinos of flavor α and β interacting with electrons, u quarks, and d quarks, normalized to the electron abundance. See refs. [23, 181, 182] for reviews on NSI. Identifying \mathbf{V}_{NSI} with the long-range matter potentials $\mathbf{V}_{e\mu}$, $\mathbf{V}_{e\tau}$, and $\mathbf{V}_{\mu\tau}$ in eq. (2.17), yields $V_{e\mu} = V_{CC}\varepsilon_{ee}$ (with $\varepsilon_{ee} = -\varepsilon_{\mu\mu}$ and $\varepsilon_{\tau\tau} = 0$), $V_{e\tau} = V_{CC}\varepsilon_{ee}$ (with $\varepsilon_{ee} = -\varepsilon_{\tau\tau}$ and $\varepsilon_{\mu\mu} = 0$), and $V_{\mu\tau} = V_{CC}\varepsilon_{\mu\mu}$ (with $\varepsilon_{\mu\mu} = -\varepsilon_{\tau\tau}$ and $\varepsilon_{ee} = 0$). Therefore, the NSI bounds $|\varepsilon_{\mu\mu} - \varepsilon_{\tau\tau}| < 0.147$ [22] translate into $V_{e\mu} < 0.147V_{CC}$, $V_{e\tau} < 0.147V_{CC}$, and $V_{\mu\tau} < 0.147V_{CC}/2$.

D Additional results under the $L_e - L_\tau$ symmetry

In the main text, we show mainly results for the $L_e - L_\mu$ and $L_\mu - L_\tau$ symmetries. Below we show results for the $L_e - L_\tau$ symmetry, under the normal mass ordering.

Figure 10 shows the oscillation probabilities as functions of the long-range matter potential, $V_{e\tau}$. Their features are similar to those for the $L_e - L_\mu$ symmetry in figure 4, except swapping $\bar{P}_{e\mu}$ and $\bar{P}_{e\tau}$.

Figure 11 shows the corresponding neutrino flavor composition at Earth. Their features track those of the oscillation probabilities in figure 10.

Figure 12 shows the posterior on $V_{e\tau}$ and limits on the coupling, $g'_{e\tau}$, obtained following the procedure described in section 4.1. The limits are similar to those for $V_{e\mu}$ under the $L_e - L_\mu$ symmetry.

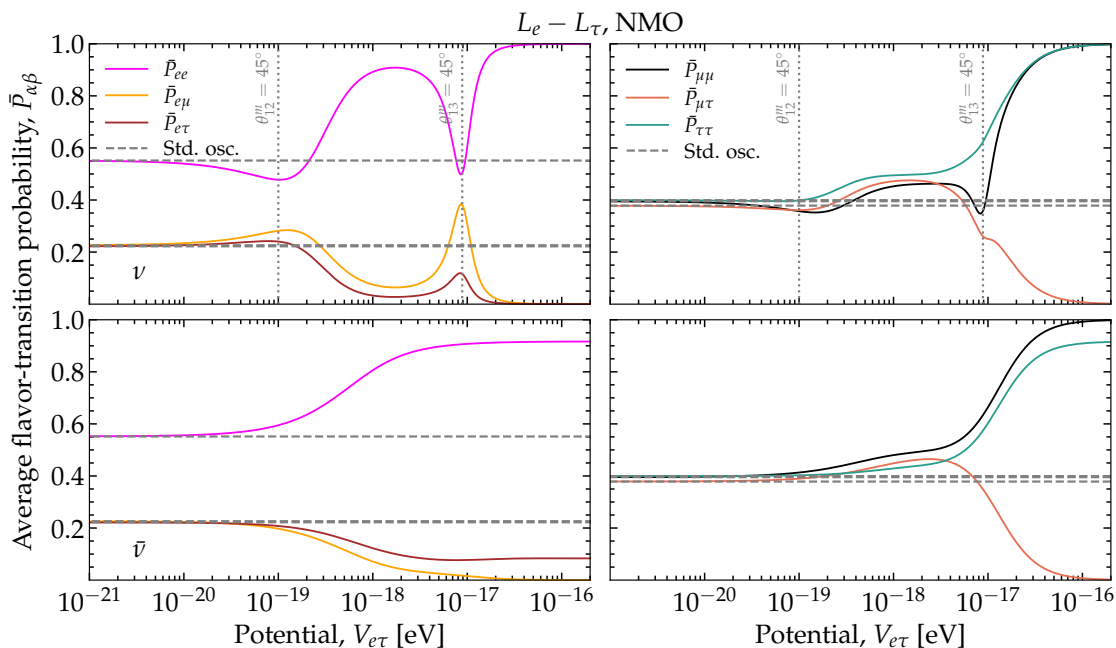


Figure 10. Average flavor-transition probabilities, eq. (2.19), as functions of the new matter potential induced by the U(1) gauge symmetry $L_e - L_\tau$. Same as figure 4, but for the $L_e - L_\tau$ symmetry. See section 2.3 and appendix D for details.

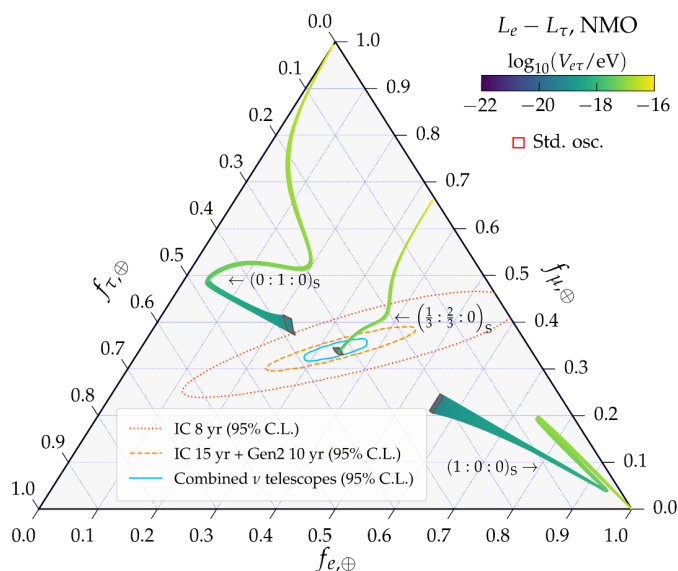


Figure 11. Flavor composition of high-energy astrophysical neutrinos at Earth, $f_{\alpha,\oplus}$, as a function of the long-range matter potential $V_{e\tau}$ under $L_e - L_\tau$. Same as figure 5, but for the $L_e - L_\tau$ symmetry. See section 3.3 and appendix D for details.

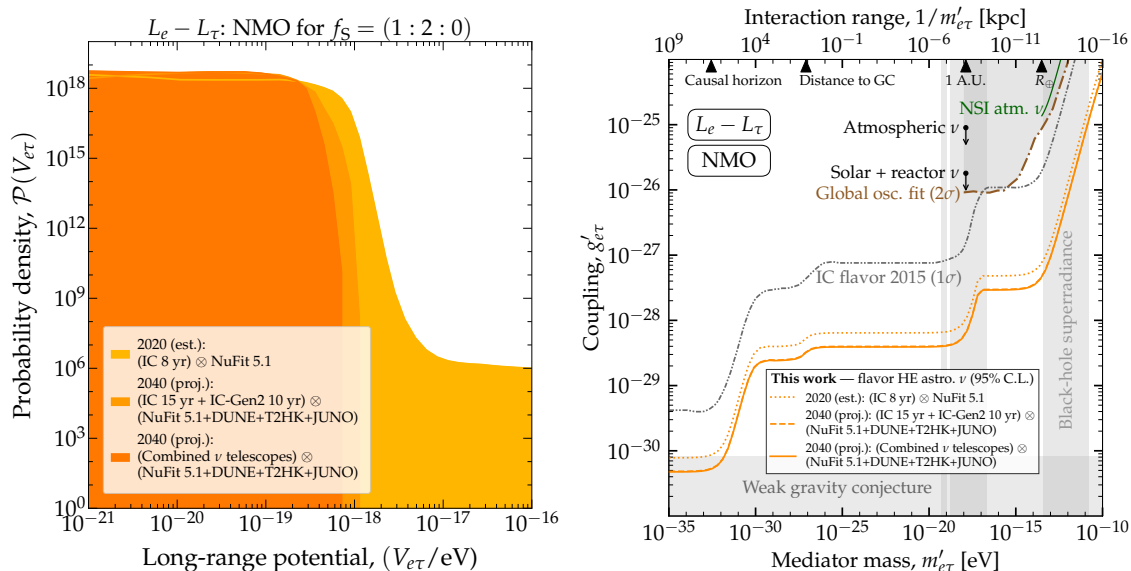


Figure 12. Constraints on the long-range matter potential $V_{e\tau}$, under the $L_e - L_\tau$ symmetry. *Left:* posterior probability density of $V_{e\tau}$. Same as figure 6, but for $V_{e\tau}$. *Right:* estimated present-day (2020) and projected (2040) upper limits (95% C.L.) on the coupling strength, $g'_{e\tau}$, of the new boson, $Z'_{e\tau}$, with mass $m'_{e\tau}$. Same as figure 8, but for $V_{e\tau}$. See section 4.2 and appendix D for details.

E Results assuming inverted neutrino mass ordering

In the main text, we show mainly results obtained assuming normal neutrino mass ordering. Below, we show results assuming inverted ordering. There are differences in the oscillation probabilities: under inverted ordering, resonant features are prominent for antineutrinos rather than for neutrinos. However, because we average the flavor composition at Earth between neutrinos and antineutrinos, the limits on the long-range matter potentials that we obtain (figure 7) are largely insensitive to the mass ordering.

Figures 13 and 14 show the oscillation probabilities as functions of the long-range matter potentials.

Figure 15 shows the corresponding neutrino flavor composition at Earth.

Figure 16 shows the posterior probability distribution of the long-range potentials, obtained following the procedure described in section 4.1.

Figure 17 shows the corresponding upper limits on the couplings, $g'_{\alpha\beta}$.

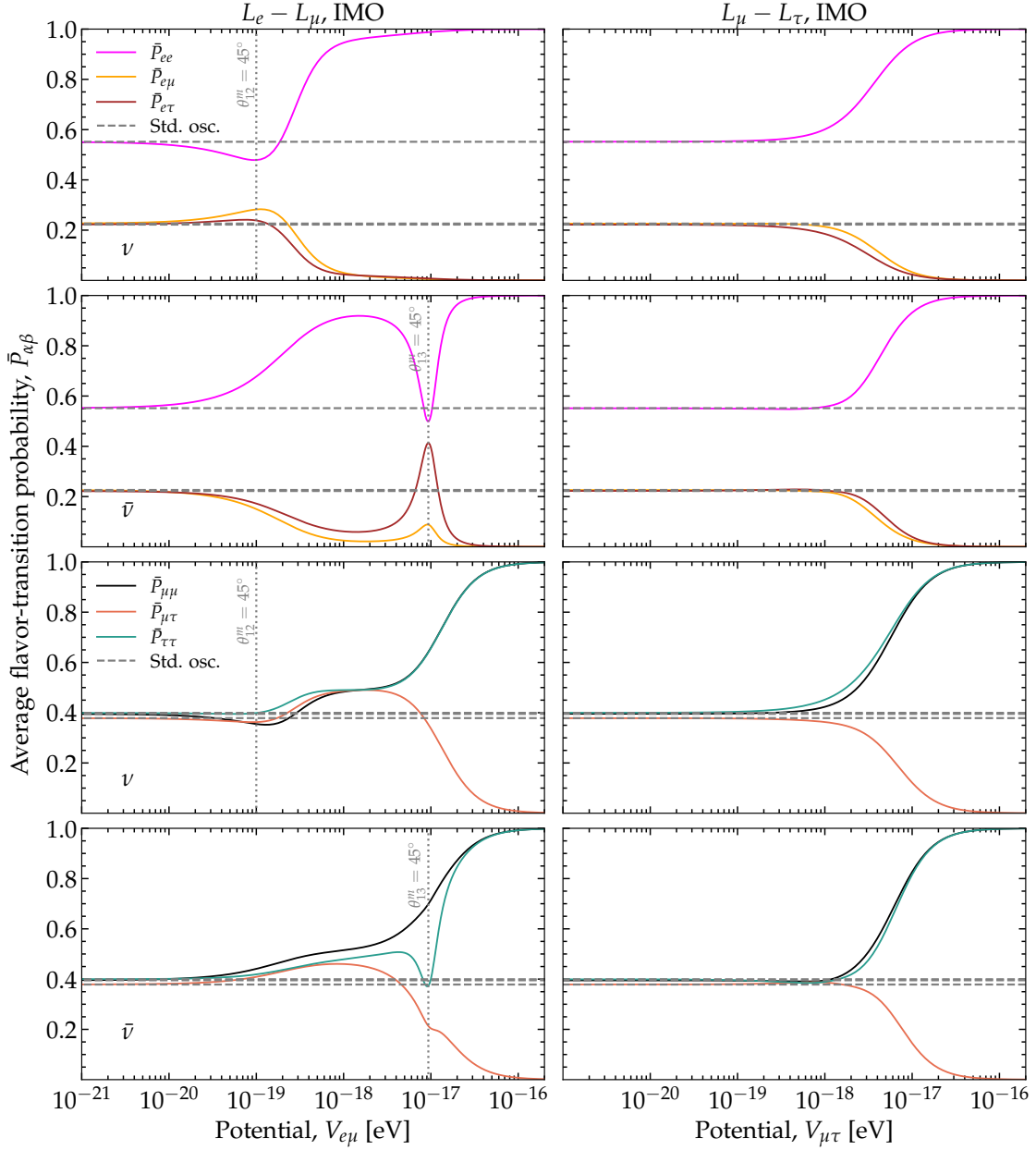


Figure 13. Average flavor-transition probabilities, eq. (2.19), as functions of the new matter potential induced by the U(1) gauge symmetries $L_e - L_\mu$ (left column) and $L_\mu - L_\tau$ (right column). Same as figure 4, but assuming inverted neutrino mass ordering (IMO). See figure 14 for the probabilities under $L_e - L_\tau$. See section 2.3 for details.

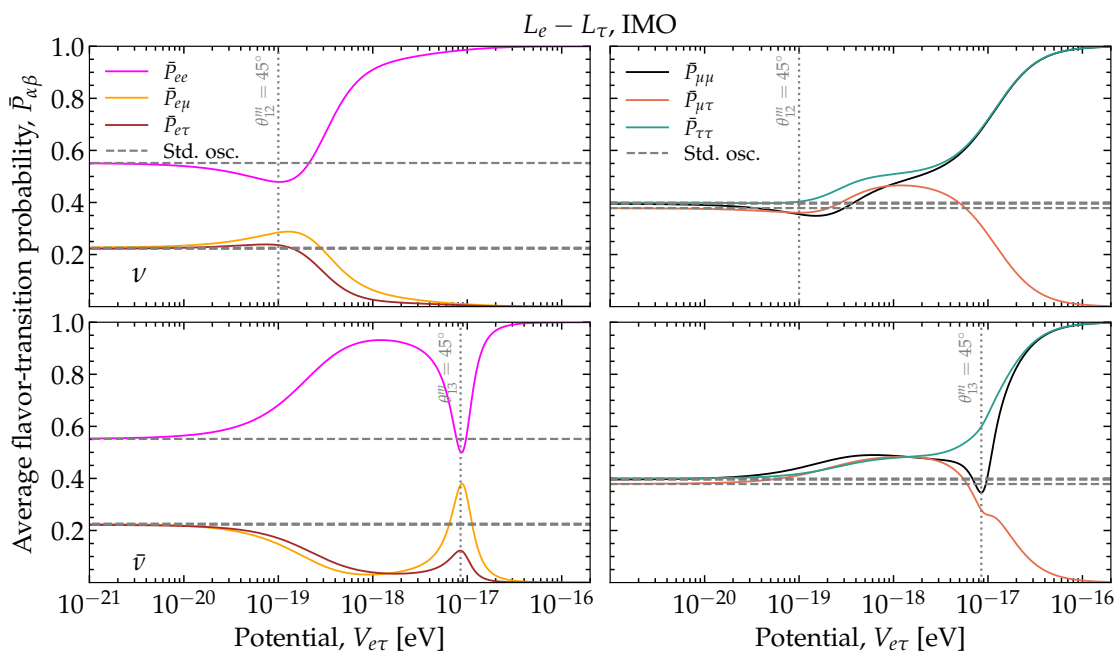


Figure 14. Average flavor-transition probabilities, eq. (2.19), as functions of the new matter potential induced by the U(1) gauge symmetry $L_e - L_\tau$. Same as figure 10, but for inverted mass ordering (IMO). See figure 13 for the probabilities under the other two symmetries. See section 2.3 for details.

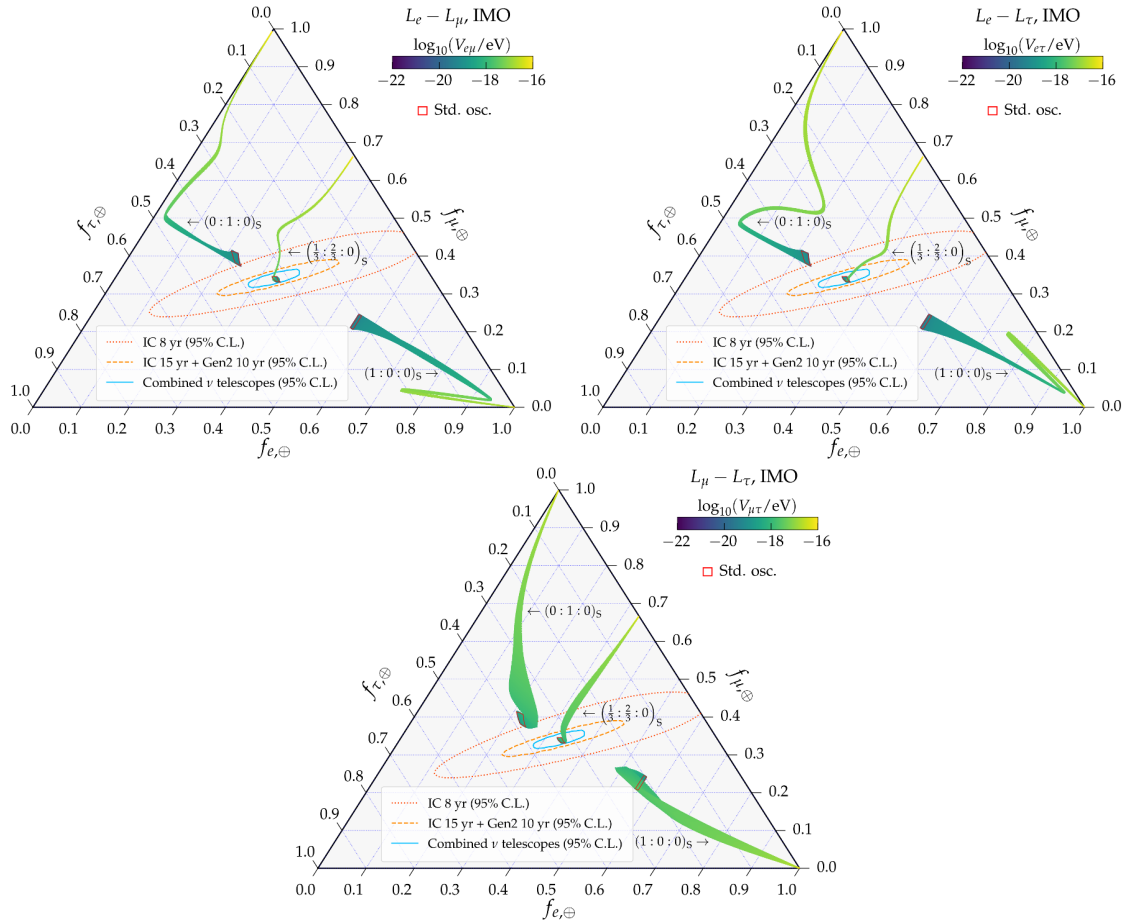


Figure 15. Flavor composition of high-energy astrophysical neutrinos at Earth, $f_{\alpha, \oplus}$, as a function of the long-range matter potential $V_{e\mu}$, under $L_e - L_{\mu}$ (top left), $V_{e\tau}$, under $L_e - L_{\tau}$ (top right), and $V_{\mu\tau}$, under $L_{\mu} - L_{\tau}$ (bottom). Same as figures 5 and 11, but for inverted mass ordering (IMO). See section 3.3 for details.

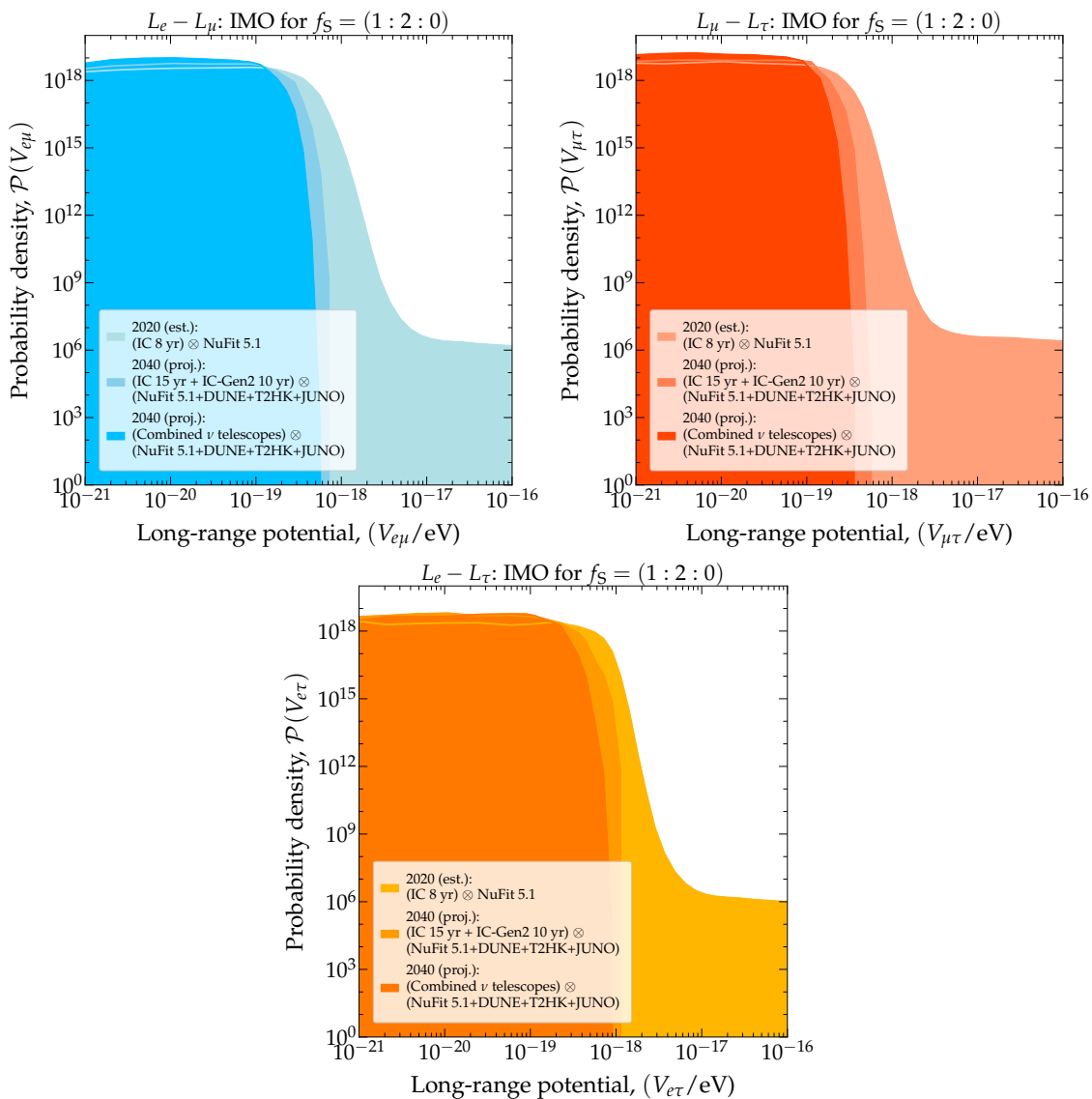


Figure 16. Posterior probability density of the long-range matter potentials $V_{e\mu}$, under $L_e - L_\mu$ (top left), $V_{e\tau}$, under $L_e - L_\tau$ (top right), and $V_{\mu\tau}$, under $L_\mu - L_\tau$ (bottom). Same as figures 6 and 12, but for inverted neutrino mass ordering (IMO). See section 4.1 for details.

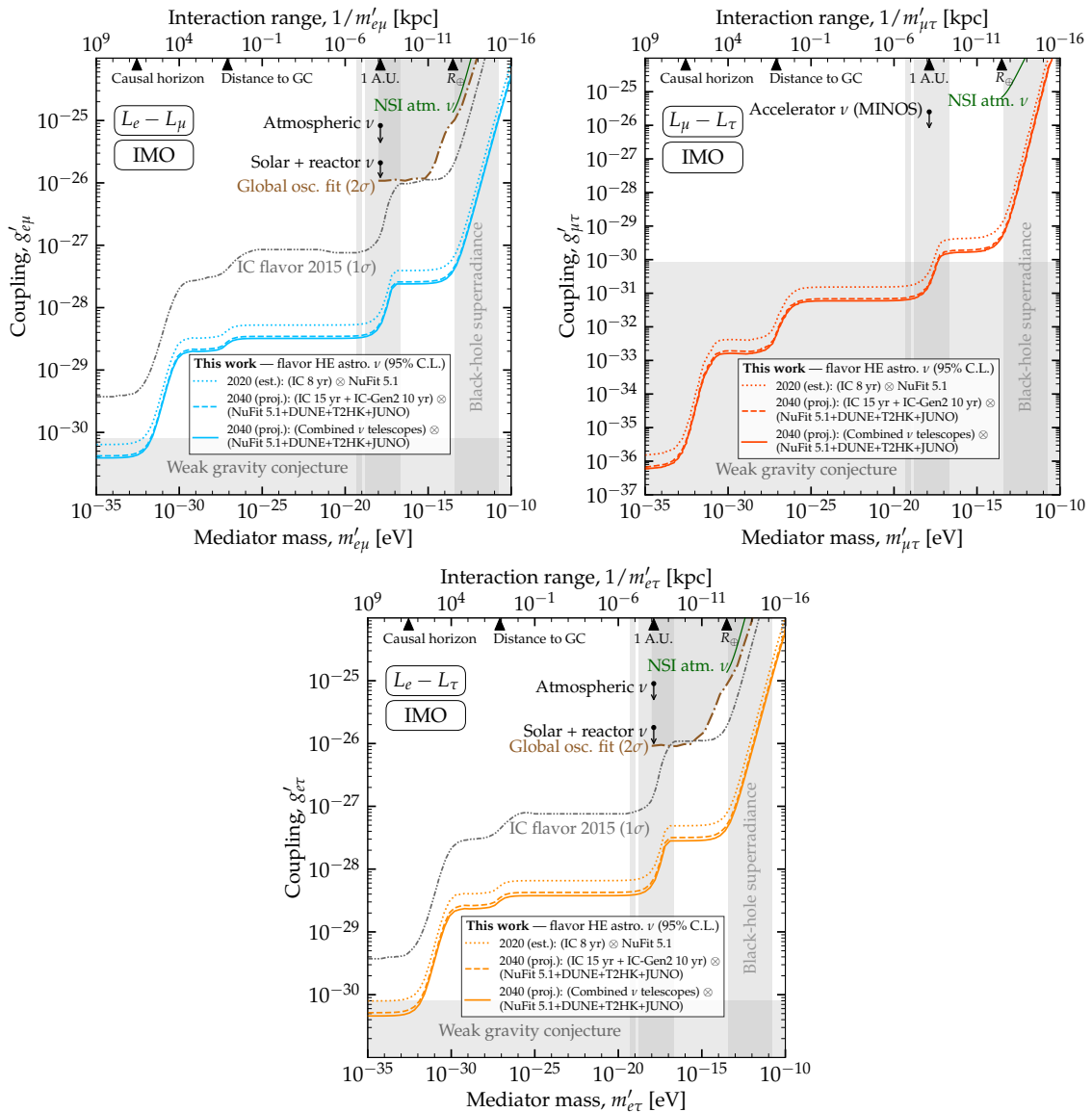


Figure 17. Estimated present-day (2020) and projected (2040) upper limits (95% C.L.) on the coupling strength, $g'_{\alpha\beta}$, of the new boson, $Z'_{\alpha\beta}$, with mass $m'_{\alpha\beta}$, that mediates flavor-dependent long-range neutrino interactions. Same as figures 8 and 12, but for inverted neutrino mass ordering (IMO). See section 4.2 for details.

Observation epoch	Upper limit (95% C.L.) on potential [10^{-19} eV]					
	$V_{e\mu}$		$V_{e\tau}$		$V_{\mu\tau}$	
	NMO	IMO	NMO	IMO	NMO	IMO
2020 (est.): IC 8 yr	3.11	2.95	4.41	4.58	1.79	1.87
2040 (proj.): IC 15 yr + Gen2 10 yr	1.11	1.28	1.69	1.93	0.731	0.837
2040 (proj.): Combined ν telescopes	1.08	1.10	1.63	1.52	0.702	0.727

Table 2. Estimated present-day (2020) and projected (2040) upper limits (95% C.L.) on the long-range matter potentials $V_{e\mu}$, $V_{e\tau}$, and $V_{\mu\tau}$. Results are for normal (NMO) and inverted neutrino mass ordering (IMO). See section 4.2 for details.

F Table of limits on the long-range potential

Table 2 shows the upper limits on the long-range matter potentials obtained in section 4.2. Figure 7 in the main text shows a graphical representation of them and figures 1, 8, 12, and 17 shows them translated into limits on the coupling, $g'_{\alpha\beta}$.

Open Access. This article is distributed under the terms of the Creative Commons Attribution License (CC-BY 4.0), which permits any use, distribution and reproduction in any medium, provided the original author(s) and source are credited.

References

- [1] ICECUBE collaboration, *First observation of PeV-energy neutrinos with IceCube*, *Phys. Rev. Lett.* **111** (2013) 021103 [[arXiv:1304.5356](#)] [[INSPIRE](#)].
- [2] ICECUBE collaboration, *Evidence for High-Energy Extraterrestrial Neutrinos at the IceCube Detector*, *Science* **342** (2013) 1242856 [[arXiv:1311.5238](#)] [[INSPIRE](#)].
- [3] ICECUBE collaboration, *Observation of High-Energy Astrophysical Neutrinos in Three Years of IceCube Data*, *Phys. Rev. Lett.* **113** (2014) 101101 [[arXiv:1405.5303](#)] [[INSPIRE](#)].
- [4] ICECUBE collaboration, *Evidence for Astrophysical Muon Neutrinos from the Northern Sky with IceCube*, *Phys. Rev. Lett.* **115** (2015) 081102 [[arXiv:1507.04005](#)] [[INSPIRE](#)].
- [5] ICECUBE collaboration, *Observation and Characterization of a Cosmic Muon Neutrino Flux from the Northern Hemisphere using six years of IceCube data*, *Astrophys. J.* **833** (2016) 3 [[arXiv:1607.08006](#)] [[INSPIRE](#)].
- [6] M. Ahlers and F. Halzen, *Opening a New Window onto the Universe with IceCube*, *Prog. Part. Nucl. Phys.* **102** (2018) 73 [[arXiv:1805.11112](#)] [[INSPIRE](#)].
- [7] ICECUBE collaboration, *The IceCube high-energy starting event sample: Description and flux characterization with 7.5 years of data*, *Phys. Rev. D* **104** (2021) 022002 [[arXiv:2011.03545](#)] [[INSPIRE](#)].
- [8] M. Ackermann et al., *High-energy and ultra-high-energy neutrinos: A Snowmass white paper*, *JHEAp* **36** (2022) 55 [[arXiv:2203.08096](#)] [[INSPIRE](#)].
- [9] T.K. Gaisser, F. Halzen and T. Stanev, *Particle astrophysics with high-energy neutrinos*, *Phys. Rept.* **258** (1995) 173 [[hep-ph/9410384](#)] [[INSPIRE](#)].

- [10] M. Ahlers, K. Helbing and C. Pérez de los Heros, *Probing Particle Physics with IceCube*, *Eur. Phys. J. C* **78** (2018) 924 [[arXiv:1806.05696](#)] [[INSPIRE](#)].
- [11] M. Ackermann et al., *Fundamental Physics with High-Energy Cosmic Neutrinos*, *Bull. Am. Astron. Soc.* **51** (2019) 215 [[arXiv:1903.04333](#)] [[INSPIRE](#)].
- [12] C.A. Argüelles et al., *Fundamental physics with high-energy cosmic neutrinos today and in the future*, *PoS ICRC2019* (2020) 849 [[arXiv:1907.08690](#)] [[INSPIRE](#)].
- [13] R. Alves Batista et al., *EuCAPT White Paper: Opportunities and Challenges for Theoretical Astroparticle Physics in the Next Decade*, [arXiv:2110.10074](#) [[INSPIRE](#)].
- [14] M. Ackermann et al., *Astrophysics Uniquely Enabled by Observations of High-Energy Cosmic Neutrinos*, *Bull. Am. Astron. Soc.* **51** (2019) 185 [[arXiv:1903.04334](#)] [[INSPIRE](#)].
- [15] ICECUBE-GEN2 collaboration, *IceCube-Gen2: the window to the extreme Universe*, *J. Phys. G* **48** (2021) 060501 [[arXiv:2008.04323](#)] [[INSPIRE](#)].
- [16] I. Esteban et al., *The fate of hints: updated global analysis of three-flavor neutrino oscillations*, *JHEP* **09** (2020) 178 [[arXiv:2007.14792](#)] [[INSPIRE](#)].
- [17] NuFIT 5.1 (2021), <http://www.nu-fit.org/>.
- [18] J. Heeck and W. Rodejohann, *Gauged $L_\mu - L_\tau$ and different Muon Neutrino and Anti-Neutrino Oscillations: MINOS and beyond*, *J. Phys. G* **38** (2011) 085005 [[arXiv:1007.2655](#)] [[INSPIRE](#)].
- [19] P. Coloma, M.C. Gonzalez-Garcia and M. Maltoni, *Neutrino oscillation constraints on $U(1)$ ' models: from non-standard interactions to long-range forces*, *JHEP* **01** (2021) 114 [*Erratum ibid.* **11** (2022) 115] [[arXiv:2009.14220](#)] [[INSPIRE](#)].
- [20] A.S. Joshipura and S. Mohanty, *Constraints on flavor dependent long range forces from atmospheric neutrino observations at super-Kamiokande*, *Phys. Lett. B* **584** (2004) 103 [[hep-ph/0310210](#)] [[INSPIRE](#)].
- [21] A. Bandyopadhyay, A. Dighe and A.S. Joshipura, *Constraints on flavor-dependent long range forces from solar neutrinos and KamLAND*, *Phys. Rev. D* **75** (2007) 093005 [[hep-ph/0610263](#)] [[INSPIRE](#)].
- [22] SUPER-KAMIOKANDE collaboration, *Study of Non-Standard Neutrino Interactions with Atmospheric Neutrino Data in Super-Kamiokande I and II*, *Phys. Rev. D* **84** (2011) 113008 [[arXiv:1109.1889](#)] [[INSPIRE](#)].
- [23] T. Ohlsson, *Status of non-standard neutrino interactions*, *Rept. Prog. Phys.* **76** (2013) 044201 [[arXiv:1209.2710](#)] [[INSPIRE](#)].
- [24] M.C. Gonzalez-Garcia and M. Maltoni, *Determination of matter potential from global analysis of neutrino oscillation data*, *JHEP* **09** (2013) 152 [[arXiv:1307.3092](#)] [[INSPIRE](#)].
- [25] ICECUBE collaboration, *A combined maximum-likelihood analysis of the high-energy astrophysical neutrino flux measured with IceCube*, *Astrophys. J.* **809** (2015) 98 [[arXiv:1507.03991](#)] [[INSPIRE](#)].
- [26] M. Bustamante and S.K. Agarwalla, *Universe's Worth of Electrons to Probe Long-Range Interactions of High-Energy Astrophysical Neutrinos*, *Phys. Rev. Lett.* **122** (2019) 061103 [[arXiv:1808.02042](#)] [[INSPIRE](#)].
- [27] M.B. Wise and Y. Zhang, *Lepton Flavorful Fifth Force and Depth-dependent Neutrino Matter Interactions*, *JHEP* **06** (2018) 053 [[arXiv:1803.00591](#)] [[INSPIRE](#)].

- [28] M. Baryakhtar, R. Lasenby and M. Teo, *Black Hole Superradiance Signatures of Ultralight Vectors*, *Phys. Rev. D* **96** (2017) 035019 [[arXiv:1704.05081](#)] [[INSPIRE](#)].
- [29] N. Arkani-Hamed, L. Motl, A. Nicolis and C. Vafa, *The String landscape, black holes and gravity as the weakest force*, *JHEP* **06** (2007) 060 [[hep-th/0601001](#)] [[INSPIRE](#)].
- [30] S.S. Chatterjee, A. Dasgupta and S.K. Agarwalla, *Exploring Flavor-Dependent Long-Range Forces in Long-Baseline Neutrino Oscillation Experiments*, *JHEP* **12** (2015) 167 [[arXiv:1509.03517](#)] [[INSPIRE](#)].
- [31] ICECUBE collaboration, *Flavor Ratio of Astrophysical Neutrinos above 35 TeV in IceCube*, *Phys. Rev. Lett.* **114** (2015) 171102 [[arXiv:1502.03376](#)] [[INSPIRE](#)].
- [32] ICECUBE collaboration, *Measurements using the inelasticity distribution of multi-TeV neutrino interactions in IceCube*, *Phys. Rev. D* **99** (2019) 032004 [[arXiv:1808.07629](#)] [[INSPIRE](#)].
- [33] ICECUBE collaboration, *Detection of astrophysical tau neutrino candidates in IceCube*, *Eur. Phys. J. C* **82** (2022) 1031 [[arXiv:2011.03561](#)] [[INSPIRE](#)].
- [34] O. Mena, S. Palomares-Ruiz and A.C. Vincent, *Flavor Composition of the High-Energy Neutrino Events in IceCube*, *Phys. Rev. Lett.* **113** (2014) 091103 [[arXiv:1404.0017](#)] [[INSPIRE](#)].
- [35] S. Palomares-Ruiz, A.C. Vincent and O. Mena, *Spectral analysis of the high-energy IceCube neutrinos*, *Phys. Rev. D* **91** (2015) 103008 [[arXiv:1502.02649](#)] [[INSPIRE](#)].
- [36] A.C. Vincent, S. Palomares-Ruiz and O. Mena, *Analysis of the 4-year IceCube high-energy starting events*, *Phys. Rev. D* **94** (2016) 023009 [[arXiv:1605.01556](#)] [[INSPIRE](#)].
- [37] R.W. Rasmussen et al., *Astrophysical neutrinos flavored with Beyond the Standard Model physics*, *Phys. Rev. D* **96** (2017) 083018 [[arXiv:1707.07684](#)] [[INSPIRE](#)].
- [38] R. Mammen Abraham et al., *Tau neutrinos in the next decade: from GeV to EeV*, *J. Phys. G* **49** (2022) 110501 [[arXiv:2203.05591](#)] [[INSPIRE](#)].
- [39] J.M. Berryman et al., *Neutrino self-interactions: A white paper*, *Phys. Dark Univ.* **42** (2023) 101267 [[arXiv:2203.01955](#)] [[INSPIRE](#)].
- [40] C.A. Argüelles et al., *Snowmass white paper: beyond the standard model effects on neutrino flavor: Submitted to the proceedings of the US community study on the future of particle physics (Snowmass 2021)*, *Eur. Phys. J. C* **83** (2023) 15 [[arXiv:2203.10811](#)] [[INSPIRE](#)].
- [41] A.G. Soto, P. Zhelmin, I. Safa and C.A. Argüelles, *Tau Appearance from High-Energy Neutrino Interactions*, *Phys. Rev. Lett.* **128** (2022) 171101 [[arXiv:2112.06937](#)] [[INSPIRE](#)].
- [42] N. Song et al., *The Future of High-Energy Astrophysical Neutrino Flavor Measurements*, *JCAP* **04** (2021) 054 [[arXiv:2012.12893](#)] [[INSPIRE](#)].
- [43] BAIKAL-GVD collaboration, *The Baikal-GVD neutrino telescope: First results of multi-messenger study*, *PoS ICRC2019* (2020) 1013 [[arXiv:1908.05450](#)] [[INSPIRE](#)].
- [44] KM3NET collaboration, *Letter of intent for KM3NeT 2.0*, *J. Phys. G* **43** (2016) 084001 [[arXiv:1601.07459](#)] [[INSPIRE](#)].
- [45] P-ONE collaboration, *The Pacific Ocean Neutrino Experiment*, *Nature Astron.* **4** (2020) 913 [[arXiv:2005.09493](#)] [[INSPIRE](#)].

- [46] A. Romero-Wolf et al., *An Andean Deep-Valley Detector for High-Energy Tau Neutrinos*, in the proceedings of the *Latin American Strategy Forum for Research Infrastructure*, (2020) [[arXiv:2002.06475](#)] [[INSPIRE](#)].
- [47] DUNE collaboration, *Deep Underground Neutrino Experiment (DUNE), Far Detector Technical Design Report, Volume I Introduction to DUNE, 2020 JINST 15 T08008* [[arXiv:2002.02967](#)] [[INSPIRE](#)].
- [48] HYPER-KAMIOKANDE collaboration, *Hyper-Kamiokande Design Report*, [arXiv:1805.04163](#) [[INSPIRE](#)].
- [49] JUNO collaboration, *Neutrino Physics with JUNO*, *J. Phys. G* **43** (2016) 030401 [[arXiv:1507.05613](#)] [[INSPIRE](#)].
- [50] ICECUBE collaboration, *Improved Characterization of the Astrophysical Muon-neutrino Flux with 9.5 Years of IceCube Data*, *Astrophys. J.* **928** (2022) 50 [[arXiv:2111.10299](#)] [[INSPIRE](#)].
- [51] R. Foot, *New Physics From Electric Charge Quantization?*, *Mod. Phys. Lett. A* **6** (1991) 527 [[INSPIRE](#)].
- [52] X.G. He, G.C. Joshi, H. Lew and R.R. Volkas, *New Z-prime phenomenology*, *Phys. Rev. D* **43** (1991) 22 [[INSPIRE](#)].
- [53] X.-G. He, G.C. Joshi, H. Lew and R.R. Volkas, *Simplest Z-prime model*, *Phys. Rev. D* **44** (1991) 2118 [[INSPIRE](#)].
- [54] R. Foot, X.G. He, H. Lew and R.R. Volkas, *Model for a light Z-prime boson*, *Phys. Rev. D* **50** (1994) 4571 [[hep-ph/9401250](#)] [[INSPIRE](#)].
- [55] R. Foot, *Avoiding the gauge hierarchy problem with see-sawed neutrino masses*, *Mod. Phys. Lett. A* **20** (2005) 3035 [[hep-ph/0505154](#)] [[INSPIRE](#)].
- [56] T. Araki et al., *Resolving the Hubble tension in a $U(1)_{L_\mu-L_\tau}$ model with the Majoron*, *PTEP* **2021** (2021) 103B05 [[arXiv:2103.07167](#)] [[INSPIRE](#)].
- [57] C.-H. Chen and T. Nomura, *Electron and muon $g-2$, radiative neutrino mass, and $\ell' \rightarrow \ell\gamma$ in a $U(1)_{e-\mu}$ model*, *Nucl. Phys. B* **964** (2021) 115314 [[arXiv:2003.07638](#)] [[INSPIRE](#)].
- [58] A. Bodas, R. Coy and S.J.D. King, *Solving the electron and muon $g-2$ anomalies in Z' models*, *Eur. Phys. J. C* **81** (2021) 1065 [[arXiv:2102.07781](#)] [[INSPIRE](#)].
- [59] P. Panda, M.K. Behera, P. Mishra and R. Mohanta, *Unveiling neutrino phenomenology, $(g-2)_{e,\mu}$ and leptogenesis through $U(1)$ gauge symmetries in an inverse seesaw model*, [arXiv:2203.14536](#) [[INSPIRE](#)].
- [60] D. Borah, M. Dutta, S. Mahapatra and N. Sahu, *Lepton anomalous magnetic moment with singlet-doublet fermion dark matter in a scotogenic $U(1)_{L_\mu-L_\tau}$ model*, *Phys. Rev. D* **105** (2022) 015029 [[arXiv:2109.02699](#)] [[INSPIRE](#)].
- [61] S. Baek, *Dark matter and muon $(g-2)$ in local $U(1)_{L_\mu-L_\tau}$ -extended Ma Model*, *Phys. Lett. B* **756** (2016) 1 [[arXiv:1510.02168](#)] [[INSPIRE](#)].
- [62] K. Asai, S. Okawa and K. Tsumura, *Search for $U(1)_{L_\mu-L_\tau}$ charged dark matter with neutrino telescope*, *JHEP* **03** (2021) 047 [[arXiv:2011.03165](#)] [[INSPIRE](#)].
- [63] G. Alonso-Álvarez, K. Bleau and J.M. Cline, *Distortion of neutrino oscillations by dark photon dark matter*, *Phys. Rev. D* **107** (2023) 055045 [[arXiv:2301.04152](#)] [[INSPIRE](#)].

- [64] T. Kumar Poddar, S. Mohanty and S. Jana, *Vector gauge boson radiation from compact binary systems in a gauged $L_\mu - L_\tau$ scenario*, *Phys. Rev. D* **100** (2019) 123023 [[arXiv:1908.09732](#)] [[INSPIRE](#)].
- [65] K. Asai, K. Hamaguchi, N. Nagata and S.-Y. Tseng, *Leptogenesis in the minimal gauged $U(1)_{L_\mu-L_\tau}$ model and the sign of the cosmological baryon asymmetry*, *JCAP* **11** (2020) 013 [[arXiv:2005.01039](#)] [[INSPIRE](#)].
- [66] C. Cesarotti, S. Homiller, R.K. Mishra and M. Reece, *Probing New Gauge Forces with a High-Energy Muon Beam Dump*, *Phys. Rev. Lett.* **130** (2023) 071803 [[arXiv:2202.12302](#)] [[INSPIRE](#)].
- [67] G. Grilli di Cortona and E. Nardi, *Probing light mediators at the MUonE experiment*, *Phys. Rev. D* **105** (2022) L111701 [[arXiv:2204.04227](#)] [[INSPIRE](#)].
- [68] G.H. Duan, X.-G. He, L. Wu and J.M. Yang, *Leptophilic dark matter in gauged $U(1)_{L_e-L_\mu}$ model in light of DAMPE cosmic ray $e^+ + e^-$ excess*, *Eur. Phys. J. C* **78** (2018) 323 [[arXiv:1711.11563](#)] [[INSPIRE](#)].
- [69] X.-G. He, *Dark Matter Annihilation Explanation for e^+e^- Excesses in Cosmic Ray*, *Mod. Phys. Lett. A* **24** (2009) 2139 [[arXiv:0908.2908](#)] [[INSPIRE](#)].
- [70] K.S. Babu, C.F. Kolda and J. March-Russell, *Implications of generalized Z - Z -prime mixing*, *Phys. Rev. D* **57** (1998) 6788 [[hep-ph/9710441](#)] [[INSPIRE](#)].
- [71] A.S. Joshipura, N. Mahajan and K.M. Patel, *Generalised μ - τ symmetries and calculable gauge kinetic and mass mixing in $U(1)_{L_\mu-L_\tau}$ models*, *JHEP* **03** (2020) 001 [[arXiv:1909.02331](#)] [[INSPIRE](#)].
- [72] S. Schlamminger et al., *Test of the equivalence principle using a rotating torsion balance*, *Phys. Rev. Lett.* **100** (2008) 041101 [[arXiv:0712.0607](#)] [[INSPIRE](#)].
- [73] E.G. Adelberger et al., *Torsion balance experiments: A low-energy frontier of particle physics*, *Prog. Part. Nucl. Phys.* **62** (2009) 102 [[INSPIRE](#)].
- [74] A.M. Dziewonski and D.L. Anderson, *Preliminary reference earth model*, *Phys. Earth Planet. Interiors* **25** (1981) 297 [[INSPIRE](#)].
- [75] P.J. McMillan, *Mass models of the Milky Way*, *Mon. Not. Roy. Astron. Soc.* **414** (2011) 2446 [[arXiv:1102.4340](#)] [[INSPIRE](#)].
- [76] M.J. Miller and J.N. Bregman, *The Structure of the Milky Way's Hot Gas Halo*, *Astrophys. J.* **770** (2013) 118 [[arXiv:1305.2430](#)] [[INSPIRE](#)].
- [77] G. Steigman, *Primordial Nucleosynthesis in the Precision Cosmology Era*, *Ann. Rev. Nucl. Part. Sci.* **57** (2007) 463 [[arXiv:0712.1100](#)] [[INSPIRE](#)].
- [78] C. Giunti and C.W. Kim, *Fundamentals of Neutrino Physics and Astrophysics*, Oxford University Press (2007) [[INSPIRE](#)].
- [79] S. Weinberg, *Cosmology*, Oxford University Press (2008) [[INSPIRE](#)].
- [80] PARTICLE DATA GROUP collaboration, *Review of Particle Physics*, *Chin. Phys. C* **38** (2014) 090001 [[INSPIRE](#)].
- [81] PLANCK collaboration, *Planck 2015 results. XIII. Cosmological parameters*, *Astron. Astrophys.* **594** (2016) A13 [[arXiv:1502.01589](#)] [[INSPIRE](#)].
- [82] D.W. Hogg, *Distance measures in cosmology*, [astro-ph/9905116](#) [[INSPIRE](#)].

- [83] A.M. Hopkins and J.F. Beacom, *On the normalisation of the cosmic star formation history*, *Astrophys. J.* **651** (2006) 142 [[astro-ph/0601463](#)] [[INSPIRE](#)].
- [84] H. Yuksel, M.D. Kistler, J.F. Beacom and A.M. Hopkins, *Revealing the High-Redshift Star Formation Rate with Gamma-Ray Bursts*, *Astrophys. J. Lett.* **683** (2008) L5 [[arXiv:0804.4008](#)] [[INSPIRE](#)].
- [85] M.D. Kistler et al., *The Star Formation Rate in the Reionization Era as Indicated by Gamma-ray Bursts*, *Astrophys. J. Lett.* **705** (2009) L104 [[arXiv:0906.0590](#)] [[INSPIRE](#)].
- [86] P.F. de Salas et al., *2020 global reassessment of the neutrino oscillation picture*, *JHEP* **02** (2021) 071 [[arXiv:2006.11237](#)] [[INSPIRE](#)].
- [87] F. Capozzi et al., *Unfinished fabric of the three neutrino paradigm*, *Phys. Rev. D* **104** (2021) 083031 [[arXiv:2107.00532](#)] [[INSPIRE](#)].
- [88] M.C. Gonzalez-Garcia, M. Maltoni and T. Schwetz, *NuFIT: Three-Flavour Global Analyses of Neutrino Oscillation Experiments*, *Universe* **7** (2021) 459 [[arXiv:2111.03086](#)] [[INSPIRE](#)].
- [89] ICECUBE et al. collaborations, *Multimessenger observations of a flaring blazar coincident with high-energy neutrino IceCube-170922A*, *Science* **361** (2018) eaat1378 [[arXiv:1807.08816](#)] [[INSPIRE](#)].
- [90] R. Stein et al., *A tidal disruption event coincident with a high-energy neutrino*, *Nature Astron.* **5** (2021) 510 [[arXiv:2005.05340](#)] [[INSPIRE](#)].
- [91] ICECUBE collaboration, *IceCube Data for Neutrino Point-Source Searches Years 2008-2018*, [arXiv:2101.09836](#) [[DOI:10.21234/CPKQ-K003](#)] [[INSPIRE](#)].
- [92] ICECUBE collaboration, *Evidence for neutrino emission from the nearby active galaxy NGC 1068*, *Science* **378** (2022) 538 [[arXiv:2211.09972](#)] [[INSPIRE](#)].
- [93] L.A. Anchordoqui et al., *Cosmic Neutrino Pevatrons: A Brand New Pathway to Astronomy, Astrophysics, and Particle Physics*, *JHEAp* **1-2** (2014) 1 [[arXiv:1312.6587](#)] [[INSPIRE](#)].
- [94] F. Halzen and A. Kheirandish, *Multimessenger Search for the Sources of Cosmic Rays Using Cosmic Neutrinos*, *Front. Astron. Space Sci.* **6** (2019) 32 [[INSPIRE](#)].
- [95] R. Alves Batista et al., *Open Questions in Cosmic-Ray Research at Ultrahigh Energies*, *Front. Astron. Space Sci.* **6** (2019) 23 [[arXiv:1903.06714](#)] [[INSPIRE](#)].
- [96] K. Murase and F.W. Stecker, *High-Energy Neutrinos from Active Galactic Nuclei*, [arXiv:2202.03381](#) [[INSPIRE](#)].
- [97] V.S. Berezinsky, P. Blasi and V.S. Ptuskin, *Clusters of Galaxies as a Storage Room for Cosmic Rays*, *Astrophys. J.* **487** (1997) 529 [[astro-ph/9609048](#)] [[INSPIRE](#)].
- [98] K. Murase, S. Inoue and S. Nagataki, *Cosmic Rays Above the Second Knee from Clusters of Galaxies and Associated High-Energy Neutrino Emission*, *Astrophys. J. Lett.* **689** (2008) L105 [[arXiv:0805.0104](#)] [[INSPIRE](#)].
- [99] K. Kotera et al., *Propagation of ultrahigh energy nuclei in clusters of galaxies: resulting composition and secondary emissions*, *Astrophys. J.* **707** (2009) 370 [[arXiv:0907.2433](#)] [[INSPIRE](#)].
- [100] K. Murase, M. Ahlers and B.C. Lacki, *Testing the Hadronuclear Origin of PeV Neutrinos Observed with IceCube*, *Phys. Rev. D* **88** (2013) 121301 [[arXiv:1306.3417](#)] [[INSPIRE](#)].

- [101] K. Fang and K. Murase, *Linking High-Energy Cosmic Particles by Black Hole Jets Embedded in Large-Scale Structures*, *Nature Phys.* **14** (2018) 396 [[arXiv:1704.00015](#)] [[INSPIRE](#)].
- [102] S. Hussain, R. Alves Batista, E.M. de Gouveia Dal Pino and K. Dolag, *High-energy neutrino production in clusters of galaxies*, *Mon. Not. Roy. Astron. Soc.* **507** (2021) 1762 [[arXiv:2101.07702](#)] [[INSPIRE](#)].
- [103] B. Paczynski and G.H. Xu, *Neutrino bursts from gamma-ray bursts*, *Astrophys. J.* **427** (1994) 708 [[INSPIRE](#)].
- [104] E. Waxman and J.N. Bahcall, *High-energy neutrinos from cosmological gamma-ray burst fireballs*, *Phys. Rev. Lett.* **78** (1997) 2292 [[astro-ph/9701231](#)] [[INSPIRE](#)].
- [105] K. Murase, K. Ioka, S. Nagataki and T. Nakamura, *High Energy Neutrinos and Cosmic-Rays from Low-Luminosity Gamma-Ray Bursts?*, *Astrophys. J. Lett.* **651** (2006) L5 [[astro-ph/0607104](#)] [[INSPIRE](#)].
- [106] M. Bustamante, P. Baerwald, K. Murase and W. Winter, *Neutrino and cosmic-ray emission from multiple internal shocks in gamma-ray bursts*, *Nature Commun.* **6** (2015) 6783 [[arXiv:1409.2874](#)] [[INSPIRE](#)].
- [107] N. Senno, K. Murase and P. Meszaros, *Choked Jets and Low-Luminosity Gamma-Ray Bursts as Hidden Neutrino Sources*, *Phys. Rev. D* **93** (2016) 083003 [[arXiv:1512.08513](#)] [[INSPIRE](#)].
- [108] T. Pitik, I. Tamborra and M. Petropoulou, *Neutrino signal dependence on gamma-ray burst emission mechanism*, *JCAP* **05** (2021) 034 [[arXiv:2102.02223](#)] [[INSPIRE](#)].
- [109] E. Guarini et al., *Multi-messenger detection prospects of gamma-ray burst afterglows with optical jumps*, *JCAP* **06** (2022) 034 [[arXiv:2112.07690](#)] [[INSPIRE](#)].
- [110] A. Loeb and E. Waxman, *The Cumulative background of high energy neutrinos from starburst galaxies*, *JCAP* **05** (2006) 003 [[astro-ph/0601695](#)] [[INSPIRE](#)].
- [111] T.A. Thompson, E. Quataert and E. Waxman, *The Starburst Contribution to the Extra-Galactic Gamma-Ray Background*, *Astrophys. J.* **654** (2006) 219 [[astro-ph/0606665](#)] [[INSPIRE](#)].
- [112] F.W. Stecker, *Are Diffuse High Energy Neutrinos from Starburst Galaxies Observable?*, *Astropart. Phys.* **26** (2007) 398 [[astro-ph/0607197](#)] [[INSPIRE](#)].
- [113] I. Tamborra, S. Ando and K. Murase, *Star-forming galaxies as the origin of diffuse high-energy backgrounds: Gamma-ray and neutrino connections, and implications for starburst history*, *JCAP* **09** (2014) 043 [[arXiv:1404.1189](#)] [[INSPIRE](#)].
- [114] A. Palladino, A. Fedynitch, R.W. Rasmussen and A.M. Taylor, *IceCube Neutrinos from Hadronically Powered Gamma-Ray Galaxies*, *JCAP* **09** (2019) 004 [[arXiv:1812.04685](#)] [[INSPIRE](#)].
- [115] E. Peretti, P. Blasi, F. Aharonian and G. Morlino, *Cosmic ray transport and radiative processes in nuclei of starburst galaxies*, *Mon. Not. Roy. Astron. Soc.* **487** (2019) 168 [[arXiv:1812.01996](#)] [[INSPIRE](#)].
- [116] E. Peretti et al., *Contribution of starburst nuclei to the diffuse gamma-ray and neutrino flux*, *Mon. Not. Roy. Astron. Soc.* **493** (2020) 5880 [[arXiv:1911.06163](#)] [[INSPIRE](#)].

- [117] A. Ambrosone et al., *Starburst galaxies strike back: a multi-messenger analysis with Fermi-LAT and IceCube data*, *Mon. Not. Roy. Astron. Soc.* **503** (2021) 4032 [[arXiv:2011.02483](#)] [[INSPIRE](#)].
- [118] N. Senno, K. Murase and P. Mészáros, *Constraining high-energy neutrino emission from choked jets in stripped-envelope supernovae*, *JCAP* **01** (2018) 025 [[arXiv:1706.02175](#)] [[INSPIRE](#)].
- [119] A. Esmaili and K. Murase, *Constraining high-energy neutrinos from choked-jet supernovae with IceCube high-energy starting events*, *JCAP* **12** (2018) 008 [[arXiv:1809.09610](#)] [[INSPIRE](#)].
- [120] P. Sarmah, S. Chakraborty, I. Tamborra and K. Auchettl, *High energy particles from young supernovae: gamma-ray and neutrino connections*, *JCAP* **08** (2022) 011 [[arXiv:2204.03663](#)] [[INSPIRE](#)].
- [121] X.-Y. Wang, R.-Y. Liu, Z.-G. Dai and K.S. Cheng, *Probing the tidal disruption flares of massive black holes with high-energy neutrinos*, *Phys. Rev. D* **84** (2011) 081301 [[arXiv:1106.2426](#)] [[INSPIRE](#)].
- [122] L. Dai and K. Fang, *Can tidal disruption events produce the IceCube neutrinos?*, *Mon. Not. Roy. Astron. Soc.* **469** (2017) 1354 [[arXiv:1612.00011](#)] [[INSPIRE](#)].
- [123] N. Senno, K. Murase and P. Meszaros, *High-energy Neutrino Flares from X-Ray Bright and Dark Tidal Disruption Events*, *Astrophys. J.* **838** (2017) 3 [[arXiv:1612.00918](#)] [[INSPIRE](#)].
- [124] C. Lunardini and W. Winter, *High Energy Neutrinos from the Tidal Disruption of Stars*, *Phys. Rev. D* **95** (2017) 123001 [[arXiv:1612.03160](#)] [[INSPIRE](#)].
- [125] B.T. Zhang, K. Murase, F. Oikonomou and Z. Li, *High-energy cosmic ray nuclei from tidal disruption events: Origin, survival, and implications*, *Phys. Rev. D* **96** (2017) 063007 [*Addendum ibid.* **96** (2017) 069902] [[arXiv:1706.00391](#)] [[INSPIRE](#)].
- [126] W. Winter and C. Lunardini, *A concordance scenario for the observed neutrino from a tidal disruption event*, *Nature Astron.* **5** (2021) 472 [[arXiv:2005.06097](#)] [[INSPIRE](#)].
- [127] S.H. Margolis, D.N. Schramm and R. Silberberg, *Ultra-high-Energy Neutrino Astronomy*, *Astrophys. J.* **221** (1978) 990 [[INSPIRE](#)].
- [128] F.W. Stecker, *Diffuse Fluxes of Cosmic High-Energy Neutrinos*, *Astrophys. J.* **228** (1979) 919 [[INSPIRE](#)].
- [129] S.R. Kelner, F.A. Aharonian and V.V. Bugayov, *Energy spectra of gamma-rays, electrons and neutrinos produced at proton-proton interactions in the very high energy regime*, *Phys. Rev. D* **74** (2006) 034018 [*Erratum ibid.* **79** (2009) 039901] [[astro-ph/0606058](#)] [[INSPIRE](#)].
- [130] A. Mucke et al., *SOPHIA: Monte Carlo simulations of photohadronic processes in astrophysics*, *Comput. Phys. Commun.* **124** (2000) 290 [[astro-ph/9903478](#)] [[INSPIRE](#)].
- [131] K. Murase and S. Nagataki, *High energy neutrino emission and neutrino background from gamma-ray bursts in the internal shock model*, *Phys. Rev. D* **73** (2006) 063002 [[astro-ph/0512275](#)] [[INSPIRE](#)].
- [132] S. Hummer, M. Ruger, F. Spanier and W. Winter, *Simplified models for photohadronic interactions in cosmic accelerators*, *Astrophys. J.* **721** (2010) 630 [[arXiv:1002.1310](#)] [[INSPIRE](#)].
- [133] S. Hummer, P. Baerwald and W. Winter, *Neutrino Emission from Gamma-Ray Burst Fireballs, Revised*, *Phys. Rev. Lett.* **108** (2012) 231101 [[arXiv:1112.1076](#)] [[INSPIRE](#)].

- [134] L. Morejon et al., *Improved photomeson model for interactions of cosmic ray nuclei*, *JCAP* **11** (2019) 007 [[arXiv:1904.07999](#)] [[INSPIRE](#)].
- [135] D. Fiorillo and M. Bustamante, *Bump-hunting in the diffuse flux of high-energy cosmic neutrinos*, *PoS ICRC2023* (2023) 999 [[arXiv:2301.00024](#)] [[INSPIRE](#)].
- [136] ICECUBE collaboration, *The IceCube Neutrino Observatory: Instrumentation and Online Systems*, *2017 JINST* **12** P03012 [[arXiv:1612.05093](#)] [[INSPIRE](#)].
- [137] ICECUBE collaboration, *Measurement of the multi-TeV neutrino cross section with IceCube using Earth absorption*, *Nature* **551** (2017) 596 [[arXiv:1711.08119](#)] [[INSPIRE](#)].
- [138] M. Bustamante and A. Connolly, *Extracting the Energy-Dependent Neutrino-Nucleon Cross Section above 10 TeV Using IceCube Showers*, *Phys. Rev. Lett.* **122** (2019) 041101 [[arXiv:1711.11043](#)] [[INSPIRE](#)].
- [139] ICECUBE collaboration, *Measurement of the high-energy all-flavor neutrino-nucleon cross section with IceCube*, [arXiv:2011.03560](#) [[DOI:10.1103/PhysRevD.104.022001](#)] [[INSPIRE](#)].
- [140] ICECUBE collaboration, *Energy Reconstruction Methods in the IceCube Neutrino Telescope*, *2014 JINST* **9** P03009 [[arXiv:1311.4767](#)] [[INSPIRE](#)].
- [141] PARTICLE DATA GROUP collaboration, *Review of Particle Physics*, *PTEP* **2022** (2022) 083C01 [[INSPIRE](#)].
- [142] J.G. Learned and S. Pakvasa, *Detecting tau-neutrino oscillations at PeV energies*, *Astropart. Phys.* **3** (1995) 267 [[hep-ph/9405296](#)] [[INSPIRE](#)].
- [143] H. Athar, G. Parente and E. Zas, *Prospects for observations of high-energy cosmic tau neutrinos*, *Phys. Rev. D* **62** (2000) 093010 [[hep-ph/0006123](#)] [[INSPIRE](#)].
- [144] S. Schonert, T.K. Gaisser, E. Resconi and O. Schulz, *Vetoing atmospheric neutrinos in a high energy neutrino telescope*, *Phys. Rev. D* **79** (2009) 043009 [[arXiv:0812.4308](#)] [[INSPIRE](#)].
- [145] T.K. Gaisser, K. Jero, A. Karle and J. van Santen, *Generalized self-veto probability for atmospheric neutrinos*, *Phys. Rev. D* **90** (2014) 023009 [[arXiv:1405.0525](#)] [[INSPIRE](#)].
- [146] S.L. Glashow, *Resonant Scattering of Antineutrinos*, *Phys. Rev.* **118** (1960) 316 [[INSPIRE](#)].
- [147] ICECUBE collaboration, *Detection of a particle shower at the Glashow resonance with IceCube*, *Nature* **591** (2021) 220 [*Erratum ibid.* **592** (2021) E11] [[arXiv:2110.15051](#)] [[INSPIRE](#)].
- [148] A. Bhattacharya, R. Gandhi, W. Rodejohann and A. Watanabe, *The Glashow resonance at IceCube: signatures, event rates and pp vs. p $\bar{\nu}$ interactions*, *JCAP* **10** (2011) 017 [[arXiv:1108.3163](#)] [[INSPIRE](#)].
- [149] A. Bhattacharya, R. Gandhi, W. Rodejohann and A. Watanabe, *On the interpretation of IceCube cascade events in terms of the Glashow resonance*, [arXiv:1209.2422](#) [[INSPIRE](#)].
- [150] D. Biehl et al., *Astrophysical Neutrino Production Diagnostics with the Glashow Resonance*, *JCAP* **01** (2017) 033 [[arXiv:1611.07983](#)] [[INSPIRE](#)].
- [151] G.-Y. Huang and Q. Liu, *Hunting the Glashow Resonance with PeV Neutrino Telescopes*, *JCAP* **03** (2020) 005 [[arXiv:1912.02976](#)] [[INSPIRE](#)].
- [152] L.J. Schumacher et al., *PLEνM: A global and distributed monitoring system of high-energy astrophysical neutrinos*, *PoS ICRC2021* (2021) 1185 [[arXiv:2107.13534](#)] [[INSPIRE](#)].

- [153] V. Brdar and R.S.L. Hansen, *IceCube Flavor Ratios with Identified Astrophysical Sources: Towards Improving New Physics Testability*, *JCAP* **02** (2019) 023 [[arXiv:1812.05541](#)] [[INSPIRE](#)].
- [154] A. Palladino, *The flavor composition of astrophysical neutrinos after 8 years of IceCube: an indication of neutron decay scenario?*, *Eur. Phys. J. C* **79** (2019) 500 [[arXiv:1902.08630](#)] [[INSPIRE](#)].
- [155] G. Barenboim and C. Quigg, *Neutrino observatories can characterize cosmic sources and neutrino properties*, *Phys. Rev. D* **67** (2003) 073024 [[hep-ph/0301220](#)] [[INSPIRE](#)].
- [156] P. Lipari, M. Lusignoli and D. Meloni, *Flavor Composition and Energy Spectrum of Astrophysical Neutrinos*, *Phys. Rev. D* **75** (2007) 123005 [[arXiv:0704.0718](#)] [[INSPIRE](#)].
- [157] S. Hummer, M. Maltoni, W. Winter and C. Yaguna, *Energy dependent neutrino flavor ratios from cosmic accelerators on the Hillas plot*, *Astropart. Phys.* **34** (2010) 205 [[arXiv:1007.0006](#)] [[INSPIRE](#)].
- [158] P. Mehta and W. Winter, *Interplay of energy dependent astrophysical neutrino flavor ratios and new physics effects*, *JCAP* **03** (2011) 041 [[arXiv:1101.2673](#)] [[INSPIRE](#)].
- [159] M. Bustamante, J.F. Beacom and W. Winter, *Theoretically palatable flavor combinations of astrophysical neutrinos*, *Phys. Rev. Lett.* **115** (2015) 161302 [[arXiv:1506.02645](#)] [[INSPIRE](#)].
- [160] C.A. Argüelles, T. Katori and J. Salvado, *New Physics in Astrophysical Neutrino Flavor*, *Phys. Rev. Lett.* **115** (2015) 161303 [[arXiv:1506.02043](#)] [[INSPIRE](#)].
- [161] A. Palladino, G. Pagliaroli, F.L. Villante and F. Vissani, *What is the Flavor of the Cosmic Neutrinos Seen by IceCube?*, *Phys. Rev. Lett.* **114** (2015) 171101 [[arXiv:1502.02923](#)] [[INSPIRE](#)].
- [162] M. Bustamante and M. Ahlers, *Inferring the flavor of high-energy astrophysical neutrinos at their sources*, *Phys. Rev. Lett.* **122** (2019) 241101 [[arXiv:1901.10087](#)] [[INSPIRE](#)].
- [163] T. Kashti and E. Waxman, *Flavoring astrophysical neutrinos: Flavor ratios depend on energy*, *Phys. Rev. Lett.* **95** (2005) 181101 [[astro-ph/0507599](#)] [[INSPIRE](#)].
- [164] M. Kachelriess and R. Tomas, *High energy neutrino yields from astrophysical sources I: Weakly magnetized sources*, *Phys. Rev. D* **74** (2006) 063009 [[astro-ph/0606406](#)] [[INSPIRE](#)].
- [165] M. Kachelriess, S. Ostapchenko and R. Tomas, *High energy neutrino yields from astrophysical sources. 2. Magnetized sources*, *Phys. Rev. D* **77** (2008) 023007 [[arXiv:0708.3047](#)] [[INSPIRE](#)].
- [166] W. Winter, *Photohadronic Origin of the TeV-PeV Neutrinos Observed in IceCube*, *Phys. Rev. D* **88** (2013) 083007 [[arXiv:1307.2793](#)] [[INSPIRE](#)].
- [167] M. Bustamante and I. Tamborra, *Using high-energy neutrinos as cosmic magnetometers*, *Phys. Rev. D* **102** (2020) 123008 [[arXiv:2009.01306](#)] [[INSPIRE](#)].
- [168] M. Bustamante, *New limits on neutrino decay from the Glashow resonance of high-energy cosmic neutrinos*, [arXiv:2004.06844](#) [[INSPIRE](#)].
- [169] P. Huber et al., *New features in the simulation of neutrino oscillation experiments with GLoBES 3.0: General Long Baseline Experiment Simulator*, *Comput. Phys. Commun.* **177** (2007) 432 [[hep-ph/0701187](#)] [[INSPIRE](#)].
- [170] DUNE collaboration, *Experiment Simulation Configurations Approximating DUNE TDR*, [arXiv:2103.04797](#) [[INSPIRE](#)].

- [171] DUNE collaboration, *Experiment Simulation Configurations Used in DUNE CDR*, [arXiv:1606.09550](#) [INSPIRE].
- [172] DUNE collaboration, *Long-baseline neutrino oscillation physics potential of the DUNE experiment*, *Eur. Phys. J. C* **80** (2020) 978 [[arXiv:2006.16043](#)] [INSPIRE].
- [173] SUPER-KAMIOKANDE collaboration, *Atmospheric neutrino oscillations with Super-Kamiokande and prospects for SuperK-Gd*, *PoS ICRC2021* (2021) 008 [INSPIRE].
- [174] DAYA BAY collaboration, *Improved Measurement of the Reactor Antineutrino Flux and Spectrum at Daya Bay*, *Chin. Phys. C* **41** (2017) 013002 [[arXiv:1607.05378](#)] [INSPIRE].
- [175] S.W. Li, M. Bustamante and J.F. Beacom, *Echo Technique to Distinguish Flavors of Astrophysical Neutrinos*, *Phys. Rev. Lett.* **122** (2019) 151101 [[arXiv:1606.06290](#)] [INSPIRE].
- [176] A. Palladino and W. Winter, *A multi-component model for observed astrophysical neutrinos*, *Astron. Astrophys.* **615** (2018) A168 [[arXiv:1801.07277](#)] [INSPIRE].
- [177] A. Capanema, A. Esmaili and K. Murase, *New constraints on the origin of medium-energy neutrinos observed by IceCube*, *Phys. Rev. D* **101** (2020) 103012 [[arXiv:2002.07192](#)] [INSPIRE].
- [178] A.D. Dolgov and G.G. Raffelt, *Screening of long range leptonic forces by cosmic background neutrinos*, *Phys. Rev. D* **52** (1995) 2581 [[hep-ph/9503438](#)] [INSPIRE].
- [179] S.I. Blinnikov, A.D. Dolgov, L.B. Okun and M.B. Voloshin, *How strong can the coupling of leptonic photons be?*, *Nucl. Phys. B* **458** (1996) 52 [[hep-ph/9505444](#)] [INSPIRE].
- [180] S.K. Agarwalla, S. Das, M. Masud and P. Swain, *Evolution of neutrino mass-mixing parameters in matter with non-standard interactions*, *JHEP* **11** (2021) 094 [[arXiv:2103.13431](#)] [INSPIRE].
- [181] O.G. Miranda and H. Nunokawa, *Non standard neutrino interactions: current status and future prospects*, *New J. Phys.* **17** (2015) 095002 [[arXiv:1505.06254](#)] [INSPIRE].
- [182] Y. Farzan and M. Tortola, *Neutrino oscillations and Non-Standard Interactions*, *Front. in Phys.* **6** (2018) 10 [[arXiv:1710.09360](#)] [INSPIRE].